



1 **Fractional relaxation noises, motions and the fractional**
2 **energy balance equation**

3
4
5
6
7
8

Shaun Lovejoy
Physics, McGill University,
3600 University st.
Montreal, Que. H3A 2T8
Canada

9 **Abstract:**

10 We consider the statistical properties of solutions of the stochastic fractional
11 relaxation equation that has been proposed as a model for the earth's energy
12 balance. In this equation, the (scaling) fractional derivative term models energy
13 storage processes that occur over a wide range of space and time scales. Up until
14 now, stochastic fractional relaxation processes have only been considered with
15 Riemann-Liouville fractional derivatives in the context of random walk processes
16 where it yields highly nonstationary behaviour. For our purposes we require the
17 stationary processes that are the solutions of the Weyl fractional relaxation
18 equations whose domain is $-\infty$ to t rather than 0 to t .

19 We develop a framework for handling fractional equations driven by white
20 noise forcings. To avoid divergences, we follow the approach used in fractional
21 Brownian motion (fBm). The resulting fractional relaxation motions (fRm) and
22 fractional relaxation noises (fRn) generalize the more familiar fBm and fGn
23 (fractional Gaussian noise). We analytically determine both the small and large
24 scale limits and show extensive analytic and numerical results on the
25 autocorrelation functions, Haar fluctuations and spectra. We display sample
26 realizations.

27 Finally, we discuss the prediction of fRn, fRm which – due to long memories is
28 a *past* value problem, not an *initial* value problem. We develop an analytic formula
29 for the fRn forecast skill and compare it to fGn. Although the large scale limit is an
30 (unpredictable) white noise that is attained in a slow power law manner, when the
31 temporal resolution of the series is small compared to the relaxation time, fRn can
32 mimic a long memory process with a wide range of exponents ranging from fGn to
33 fBm and beyond. We discuss the implications for monthly, seasonal, annual
34 forecasts of the earth's temperature as well as for projecting the temperature to
35 2050 and 2100.

36 **1. Introduction:**

37 Over the last decades, stochastic approaches have rapidly developed and have
38 spread throughout the geosciences. From early beginnings in hydrology and
39 turbulence, stochasticity has made inroads in many traditionally deterministic areas.



40 This is notably illustrated by stochastic parametrisations of Numerical Weather
41 Prediction models, e.g. [Buizza *et al.*, 1999], and the “random” extensions of
42 dynamical systems theory, e.g. [Chekroun *et al.*, 2010].

43 Pure stochastic approaches have developed primarily along two distinct lines.
44 One is the classical (integer ordered, linear) stochastic differential equation
45 approach based the Itô calculus that goes back to the 1950’s (see the useful review
46 [Dijkstra, 2013]). The other is the scaling strand that encompasses both linear
47 (monofractal, [Mandelbrot, 1982]) and nonlinear (multifractal) models (see the
48 review [Lovejoy and Schertzer, 2013]). These and other stochastic approaches have
49 played important roles in nonlinear Geoscience.

50 Up until now, the scaling and differential equation strands of stochasticity have
51 had surprisingly little overlap. This is at least partly for technical reasons: integer
52 ordered stochastic differential equations have exponential Green’s functions that
53 are incompatible with wide range scaling. However, this shortcoming can – at least
54 in principle - be easily overcome by introducing at least some derivatives of
55 fractional order. Once the (typically) ad hoc restriction to integer orders is dropped,
56 the Green’s functions are “generalized exponentials” and these are based instead on
57 power laws (see the review [Podlubny, 1999]). The integer ordered equations that
58 have received most attention are thus exceptional special, nonscaling, cases.

59 Under the title “Fractal operators” [West *et al.*, 2003], review and emphasize
60 that in order to yield scaling behaviours, it suffices that stochastic differential
61 equations contain fractional derivatives. However, when it is the time derivatives
62 that are fractional, the relevant processes are generally non-Markovian [Jumarie,
63 1993], so that there is no Fokker-Plank (FP) equation describing the probabilities of
64 the corresponding fractional Langevin equation (see however [Schertzer *et al.*,
65 2001] for fractional spatial partial derivative equations). Furthermore, we expect
66 that - as with the simplest scaling stochastic model – fractional Brownian motion
67 (fBm, [Mandelbrot and Van Ness, 1968]) - that the solutions will not be semi-
68 Martingales and hence that the Itô calculus used for integer ordered equations will
69 not be applicable (see [Biagini *et al.*, 2008]).

70 In this paper, we consider the fractional energy balance equation (FEBE)
71 which is a stochastic fractional relaxation equation ([Lovejoy *et al.*, 2019]). The
72 FEBE is a model of the earth’s global temperature where the key energy storage
73 processes are modelled by a fractional time derivative term. The FEBE differs from
74 the classical energy balance equation (EBE) in several ways. Whereas the EBE is
75 integer ordered and describes the deterministic, exponential relaxation of the
76 earth’s temperature to thermodynamic equilibrium (Newton’s law of cooling), the
77 FEBE is both stochastic and of fractional order. The FEBE unites the forcings due
78 internal and external variabilities: the former is treated as a zero mean noise and
79 the latter as the deterministic ensemble average of the total forcing. Physically, in
80 the EBE the earth’s energy storage is modelled by a uniform slab of material
81 whereas in the FEBE, it is instead modelled by a scaling hierarchy of storage
82 mechanisms so that the temperature relaxes to equilibrium in a power law rather
83 than exponential manner.

84 An important but less obvious EBE - FEBE difference is that whereas the
85 former is an *initial* value problem whose initial condition is the earth’s temperature



86 at $t = 0$, the FEBE is effectively a *past* value problem whose prediction skill improves
87 with the amount of available past data and - depending on the parameters - it can
88 have an enormous memory. To understand this, we recall that an important aspect
89 of fractional derivatives is that they are defined as convolutions over various
90 domains. To date, the main one that has been applied to physical problems is the
91 Riemann-Liouville (RL) fractional derivative in which the domain of the convolution
92 is the interval between an initial time = 0 and a later time t . This is the exclusive
93 domain considered in Podlubny's mathematical monograph on deterministic
94 fractional differential equations [Podlubny, 1999] as well as in the stochastic
95 fractional physics discussed in [West *et al.*, 2003]. A key point of the FEBE is that it
96 is instead based on Weyl fractional derivatives i.e. derivatives defined over semi-
97 infinite domains, here from $-\infty$ to t .

98 The purpose of this paper is to understand various statistical properties of the
99 solutions of noise driven Weyl fractional differential equations. We focus on the
100 Weyl fractional relaxation equation that underpins the FEBE, particularly its
101 stationary noise solution - "fractional Relaxation noise" (fRn) - and the fRn integral
102 "fractional Relaxation motion" (fRm). These are direct extensions of the widely
103 studied fractional Gaussian noise (fGn) and fractional Brownian motion (fBm)
104 processes. We derive the main statistical properties of both fRn and fRm including
105 spectra, correlation functions and (stochastic) predictability limits needed for
106 forecasting the earth temperature ([Lovejoy *et al.*, 2015], [Del Rio Amador and
107 Lovejoy, 2019]) or projecting it to 2050 or 2100 [Hébert *et al.*, 2019].

108 2. Unified treatment of fBm and fRm:

109 2.1 fRn, fRm, fGn and fBm

110 [Lovejoy *et al.*, 2019] argued that the earth's global energy balance could be
111 well modelled by the (linearized) fractional energy balance equation. Taking T as
112 the globally averaged temperature, τ as the characteristic time scale for energy
113 storage/relaxation processes and F as the (stochastic) forcing, the FEBE can be
114 written in Langevin form as:

$$115 \tau^H \left({}_a D_t^H T \right) + T = F \quad (1)$$

116 Where (for $0 < H < 1$) the fractional derivative symbol ${}_a D_t^H$ is defined as:

$$117 {}_a D_t^H T = \frac{1}{\Gamma(1-H)} \int_a^t (t-s)^{H-1} T'(s) ds; \quad T' = \frac{dT}{ds} \quad (2)$$

118 Derivatives of order $\nu > 1$ can be obtained using $\nu = H + m$ where m is the integer part
119 of ν , and then applying this formula to the m^{th} ordinary derivative. The main case

120 studied in applications is $a = 0$; the "Riemann-Liouville fractional derivative" ${}_0 D_t^H$,

121 here we will be interested in $a = -\infty$; the "Weyl fractional derivative" ${}_{-\infty} D_t^H$.



122 Since equation 1 is linear, by taking ensemble averages, it can be decomposed
123 into deterministic and random components with, the former driven by the mean
124 forcing $\langle F \rangle$ - representing the forcing external to system - and the latter by the
125 stochastic fluctuating component $F - \langle F \rangle$ representing the forcing due to the internal
126 variability. In [Lovejoy *et al.*, 2019] we primarily considered the deterministic part,
127 in the following, we consider the simplest purely stochastic model in which $\langle F \rangle = 0$
128 and $F = \gamma$ where γ is a Gaussian “delta correlated” white noise:

$$\langle \gamma(s) \rangle = 0; \quad \langle \gamma(s) \gamma(u) \rangle = \delta(s - u) \quad (3)$$

129
130 In [Hébert *et al.*, 2019] it was argued on the basis of an empirical study of ocean-
131 atmosphere coupling that $\tau \approx 2$ years and in [Lovejoy *et al.*, 2019] and [Del Rio
132 Amador and Lovejoy, 2019] that the value $H \approx 0.4$ reproduced both the earth’s
133 temperature both at scales $\gg \tau$ as well as for macroweather scales (longer than the
134 weather regime scales of about 10 days) but still $< \tau$.

135 When $0 < H < 1$, eq. 1 with $\gamma(t)$ replaced by a deterministic forcing is a
136 fractional generalization of the usual ($H = 1$) relaxation equation; when $1 < H < 2$, it
137 is a generalization of the usual ($H = 2$) oscillation equation, the “fractional oscillation
138 equation”, see e.g. [Podlubny, 1999]. This classification is based on the deterministic
139 equations; for the noise driven equations, we find that there are two critical
140 exponents $H = 1/2$ and $H = 3/2$ and hence three ranges. Although we focus on the
141 range $0 < H < 3/2$ (especially $0 < H < 1/2$), we also give results for the full range $0 <$
142 $H < 2$ that includes the oscillation range.

143 To simplify the development, we use the relaxation time τ to
144 nondimensionalize time i.e. to replace time by t/τ to obtain the canonical Weyl
145 fractional relaxation equation:

$$146 \quad ({}_{-\infty}D_t^H + 1)U_H = \gamma(t); \quad U_H = \frac{dQ_H}{dt} \quad (4)$$

147 for the process U_H . The dimensional solution of eq. 1 with $F = \gamma$ is simply $T(t) = \tau^{-1}$
148 $U_H(t/\tau)$ so that in the nondimensional eq. 4, the characteristic transition “relaxation”
149 time between dominance by the high frequency (differential) and the low frequency
150 (U_H term) is $t = 1$. Although we give results for the full range $0 < H < 2$ - i.e. both the
151 “relaxation” and “oscillation” ranges - for simplicity, we refer to the solution $U_H(t)$
152 as “fractional Relaxation noise” (fRn) and to $Q_H(t)$ as “fractional Relaxation motion”
153 (fRm). Note that we take $Q_H(0) = 0$ so that Q_H is related to U_H via an ordinary
154 integral from time = 0 to t and that fRn is only strictly a noise when $H \leq 1/2$.

155 In dealing with fRn and fRm, we must be careful of various small and large t
156 divergences. For example, eqs. 1 and 4 are the fractional Langevin equations
157 corresponding to generalizations of integer ordered stochastic diffusion equations:
158 the solution with the classical $H = 1$ value is the Ohenstein-Uhlenbeck process. Since
159 $\gamma(t)$ is a “generalized function” - a “noise” - it does not converge at a mathematical
160 instant in time, it is only strictly meaningful under an integral sign. Therefore, a
161 more standard form of eq. 4 is obtained by integrating both sides by order H :



$$U_H(t) = - {}_{-\infty}D_t^{-H}U_H + {}_{-\infty}D_t^{-H}\gamma = -\frac{1}{\Gamma(H)}\int_{-\infty}^t(t-s)^{H-1}U_H(s)ds + \frac{1}{\Gamma(H)}\int_{-\infty}^t(t-s)^{H-1}\gamma(s)ds \quad (5)$$

162
 163

164 The white noise forcing in the above is statistically stationary; we show below that
 165 the solution for $U_H(t)$ is also statistically stationary. It is tempting to obtain an
 166 equation for the motion $Q_H(t)$ by integrating eq. 4 from $-\infty$ to t to obtain the
 167 fractional Langevin equation: ${}_{-\infty}D_t^H Q_H + Q_H = W$ where W is Wiener process (a usual
 168 Brownian motion) satisfying $dW = \gamma(t)dt$. Unfortunately the Wiener process
 169 integrated $-\infty$ to t almost surely diverges, hence we relate Q_H to U_H by an integral
 170 from 0 to t .

171 fRn and fRm are generalizations of fractional Gaussian noise (fGn, F_H) and
 172 fractional Brownian motion (fBm, B_H); this can be seen since the latter satisfy the
 173 simpler fractional Langevin equation:

$${}_{-\infty}D_t^H F_H = \gamma(t); \quad F_H = \frac{dB_H}{dt} \quad (6)$$

174
 175 so that F_H is a Weyl fractional integration of order H of a white noise and if $H = 0$,
 176 then F_H itself is a white noise and B_H is it's ordinary integral (from time = 0 to t), a
 177 usual Brownian motion, it satisfies $B_H(0) = 0$ (F_H is not to be confused with the
 178 forcing F).

179 Before continuing, a comment is necessary on the use of the symbol H that
 180 Mandelbrot introduced for fBm in honour of E. Hurst's pioneering study of long
 181 memory processes in Nile flooding [Hurst, 1951]. First, note that eq. 6 implies that
 182 the root mean square (RMS) increments of B_H over intervals Δt grow as

183 $\langle \Delta B_H(\Delta t)^2 \rangle^{1/2} \propto \Delta t^{H+1/2}$ (see below). Since fBm is often defined by this scaling

184 property, it is usual to use the fBm exponent $H_B = H+1/2$. In terms of H_B , from eq. 6,
 185 we see that fGn (F_H) is a fractional integration of a white noise of order $H = H_B - 1/2$,
 186 whereas fBm is an integral of order $H_B + 1/2$, the $1/2$ being a consequence of the
 187 fundamental scaling of the Wiener measure whose density is $\gamma(t)$. While the
 188 parametrization in terms of H_B is convenient for fGn and fBm, in this paper, we
 189 follow [Schertzer and Lovejoy, 1987] who more generally used H to denote an order
 190 of fractional integration. This more general usage includes the use of H as a general
 191 order of fractional integration in the Fractionally Integrated Flux (FIF) model
 192 [Schertzer and Lovejoy, 1987] which is the basis of space-time multifractal modelling
 193 (see the monograph [Lovejoy and Schertzer, 2013]). In the FIF generalization, the
 194 density of a Wiener measure (i.e. the white noise forcing in eq. 6) is replaced by the
 195 density of a (conservative) multifractal measure. The scaling of this multifractal
 196 measure is different from that of the Wiener measure so that the extra $1/2$ term
 197 does not appear. A consequence is that in multifractal processes, H simultaneously
 198 characterizes the order of fractional differentiation/integration ($H < 0$ or $H > 0$), and
 199 has a straightforward empirical interpretation as the "fluctuation exponent" that
 200 characterizes the rate at which fluctuations grow ($H > 0$) or decay ($H < 0$) with scale.



201 In comparison, for fBm, the critical H distinguishing integration and differentiation
 202 is still zero, but $H > 0$ or $H < 0$ corresponds to fluctuation exponents $H_B > 1/2$ or H_B
 203 $< 1/2$; which for these Gaussian processes is termed “persistence” and
 204 antipersistence”. There are therefore several H 's in the literature and in the paper we
 205 continue to denote the order of the fractional integration by H but we relate it to
 206 other exponents as needed.

207 2.2 Green's functions

208 As usual, we can solve inhomogeneous linear differential equations by using
 209 appropriate Green's functions:

$$210 \quad F_H(t) = \int_{-\infty}^t G_{0,H}^{(fGn)}(t-s)\gamma(s)ds \quad (7)$$

$$211 \quad U_H(t) = \int_{-\infty}^t G_{0,H}^{(fRn)}(t-s)\gamma(s)ds$$

211 Where $G_{0,H}^{(fGn)}$ and $G_{0,H}^{(fRn)}$ are Green's functions for the differential operators
 212 corresponding respectively to ${}_{-\infty}D_t^H$ and ${}_{-\infty}D_t^H + 1$.

213 $G_{0,H}^{(fGn)}$ and $G_{0,H}^{(fRn)}$ are the usual “impulse” (Dirac) response Green's functions
 214 (hence the subscript “0”). For the differential operator Ξ they satisfy:

$$215 \quad \Xi G_{0,H}(t) = \delta(t) \quad (8)$$

216 Integrating this equation we find an equation for their integrals $G_{1,H}$ which are thus
 217 “step” (Heaviside, subscript “1”) response Green's functions satisfying:

$$218 \quad \Xi G_{1,H}(t) = \Theta(t); \quad \Theta(t) = \int_{-\infty}^t \delta(s)ds \quad ;$$

$$219 \quad \frac{dG_{1,H}}{dt} = G_{0,H} \quad (9)$$

221 where Θ is the Heaviside (step) function. The inhomogeneous equation:

$$222 \quad \Xi f(t) = F(t) \quad (10)$$

223 has a solution in terms of either an impulse or a step Green's function:

$$224 \quad f(t) = \int_{-\infty}^t G_{0,H}(t-s)F(s)ds = \int_{-\infty}^t G_{1,H}(t-s)F'(s)ds \quad (11)$$

225 the equivalence being established by integration by parts with the conditions
 226 $F(-\infty) = 0$ and $G_{1,H}(0) = 0$.

227 For fGn, the Green's functions are simply the kernels of Weyl fractional
 228 integrals:

$$229 \quad F_H(t) = \frac{1}{\Gamma(H)} \int_{-\infty}^t (t-s)^{H-1} \gamma(s)ds \quad (12)$$



230 obtained by integrating both sides of eq. 6 by order H . We conclude:

$$\begin{aligned}
 G_{0,H}^{(fGn)} &= \frac{t^{H-1}}{\Gamma(H)}; \\
 G_{1,H}^{(fGn)} &= \frac{t^H}{\Gamma(H+1)};
 \end{aligned}
 \quad -\frac{1}{2} \leq H < \frac{1}{2}
 \tag{13}$$

232 Similarly, appendix A shows that for fRn, due to the statistical stationarity of the
 233 white noise forcing $\gamma(t)$, that the Riemann-Liouville Green's functions can be used:

$$U_H(t) = \int_{-\infty}^t G_{0,H}^{(fRn)}(t-s)\gamma(s)ds
 \tag{14}$$

235 with:

$$\begin{aligned}
 G_{0,H}^{(fRn)}(t) &= \sum_{n=1}^{\infty} (-1)^{n+1} \frac{t^{nH-1}}{\Gamma(nH)} \\
 G_{1,H}^{(fRn)}(t) &= \sum_{n=1}^{\infty} (-1)^{n+1} \frac{t^{nH}}{\Gamma(nH+1)}
 \end{aligned}
 \quad 0 < H \leq 2
 \tag{15}$$

237 so that $G_{0,H}^{(fGn)}$, $G_{1,H}^{(fGn)}$ are simply the first terms in the power series expansions of the
 238 corresponding fRn, fRm Green's functions. These Green's functions are often
 239 equivalently written in terms of Mittag-Leffler functions, $E_{\alpha,\beta}$:

$$\begin{aligned}
 G_{0,H}^{(fRn)}(t) &= t^{H-1} E_{H,H}(-t^H) & E_{\alpha,\beta}(z) &= \sum_{k=0}^{\infty} \frac{z^k}{\Gamma(\alpha k + \beta)} \\
 G_{1,H}^{(fRn)}(t) &= t^H E_{H,H+1}(-t^H) & & H \geq 0
 \end{aligned}
 \tag{16}$$

241 By taking integer H , the Γ functions reduce to factorials and $G_{0,H}$, $G_{1,H}$ reduce to
 242 exponentials hence, $G_{0,H}^{(fRn)}$, $G_{1,H}^{(fRn)}$ are sometimes called "generalized exponentials".
 243 Finally, we note that at the origin, for $0 < H < 1$, $G_{0,H}$ is singular whereas $G_{1,H}$ is
 244 regular so that it is often advantageous to use the latter (step) response function.
 245 These Green's functions are shown in figure 1. When $0 < H \leq 1$, the step response is
 246 monotonic; in an energy balance model, this would correspond to relaxation to
 247 thermodynamic equilibrium. When $1 < H < 2$, we see that there is overshoot and
 248 oscillations around the long term value.

250 In order to understand the relaxation process - i.e. the approach to asymptotic
 251 value 1 in fig. 1 for the step response $G_{1,H}$ - we need the asymptotic expansions:

$$G_{0,H}^{(fRn)}(t) = H \sum_{n=1}^{\infty} (-1)^{n+1} \frac{t^{-1-nH}}{\Gamma(1-nH)}; \quad t \gg 1$$

252

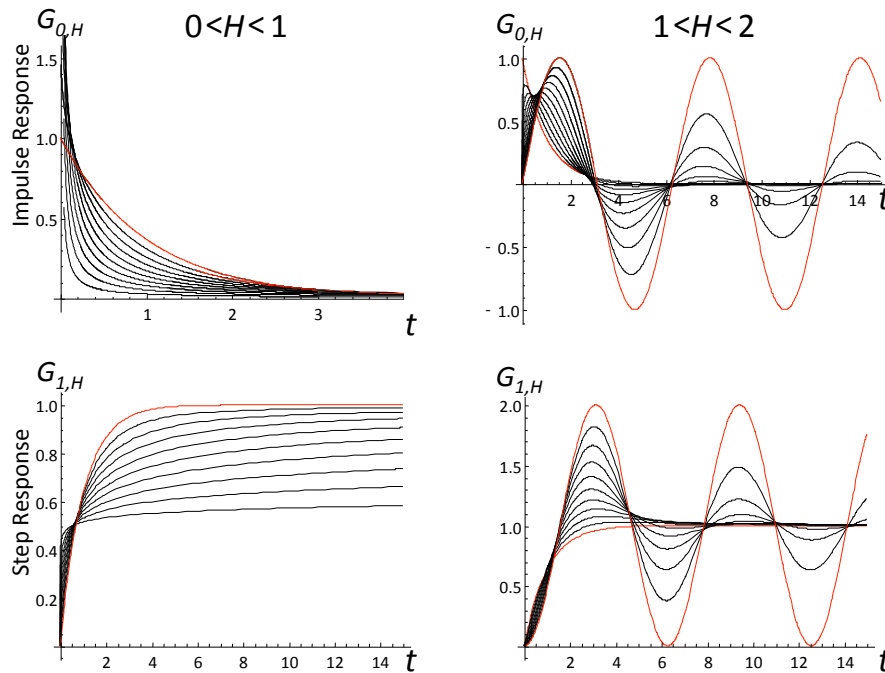


$$G_{1,H}^{(fRn)}(t) = 1 + \sum_{n=1}^{\infty} (-1)^n \frac{t^{-nH}}{n\Gamma(1-nH)}; \quad t \gg 1 \quad (17)$$

253
 254 $(0 < H < 1, 1 < H < 2)$ [Podlubny, 1999], i.e. power laws in t^H rather than t^H .
 255 According to this, the asymptotic approach to the step function response (bottom
 256 row in fig. 1) is a slow, power law process. In the FEBE, this implies for example
 257 that the classical CO₂ doubling experiment would yield a power law rather than
 258 exponential approach to a new thermodynamic equilibrium. Comparing this to the
 259 EBE – i.e. the special case $H = 1$ – we have:

$$G_{0,1}(t) = e^{-t}; \quad G_{1,1}(t) = 1 - e^{-t} \quad (18)$$

261 so that when $H = 1$, the asymptotic step response is instead approached
 262 exponentially fast. There are also analytic formulae for fRn when $H = 1/2$ discussed
 263 in appendix C notably involving logarithmic corrections.



264
 265 Fig. 1: The impulse (top) and step response functions (bottom) for the fractional relaxation
 266 range $(0 < H < 1, \text{left, red is } H = 1, \text{the exponential})$, the black curves, bottom to top are for H
 267 $= 1/10, 2/10, \dots, 9/10)$ and the fractional oscillation range $(1 < H < 2, \text{red are the integer}$
 268 $\text{values } H = 1, \text{bottom, the exponential, and top, } H = 2, \text{the sine function, the black curves,}$
 269 $\text{bottom to top are for } H = 11/10, 12/10, \dots, 19/10)$.



270 **2.3 A family of Gaussian noises and motions:**

271 In the above, we discussed fGn, fRn and their integrals fBm, fRm, but these are
 272 simply special cases of a more general theory valid for a wide family of Green's
 273 functions that lead to convergent noises and motions. We expect for example that
 274 our approach also applies to the stochastic Basset's equation discussed in
 275 [Karczewska and Lizama, 2009], which could be regarded as an extension of the
 276 stochastic relaxation equation. With the motivation outlined in the previous
 277 sections, the simplest way to proceed is to start by defining the general motion $Z_H(t)$
 278 as:

279
$$Z_H(t) = N_H \int_{-\infty}^t G_{1,H}(t-s)\gamma(s)ds - N_H \int_{-\infty}^0 G_{1,H}(-s)\gamma(s)ds \quad (19)$$

280 where N_H is a normalization constant and H is an index. It is advantageous to
 281 rewrite this in standard notation (e.g. [Biagini et al., 2008]) as:

282
$$Z_H(t) = N_H \int_{\mathbb{R}} (G_{1,H}(t-s)_+ - G_{1,H}(-s)_+) \gamma(s) ds \quad (20)$$

283 where the "+" subscript indicates that the argument is > 0 , and the range of
 284 integration is over all the real axis \mathbb{R} . Here and throughout, the Green's functions
 285 need only be specified for $t>0$ corresponding to their causal range.

286 The advantage of starting with the motion Z_H is that it is based on the step
 287 response $G_{1,H}$ which is finite at small t ; the disadvantage is that integrals may
 288 diverge at large scales. The second (constant) term in eq. 20 was introduced by
 289 [Mandelbrot and Van Ness, 1968] for fBm precisely in order to avoid large scale
 290 divergences in fBm. As discussed in appendix A, the introduction of this constant
 291 physically corresponds to considering the long time behaviour of the fractional
 292 random walks discussed in [Kobayev and Romanov, 2000] and [West et al., 2003].
 293 The physical setting of the random walk applications is a walker with position $X(t)$
 294 and velocity $V(t)$. Assuming that the walker starts at the origin corresponds to a
 295 fractionally diffusing particle obeying the fractional Riemann-Liouville relaxation
 296 equation.

297 From the definition (eq. 19 or 20), we have:

298
$$\langle Z_H(0) \rangle = 0; \quad Z_H(0) = 0 \quad (21)$$

299 Hence, the origin plays a special role, so that the $Z_H(t)$ process is nonstationary.

300 The variance $V_H(t)$ of Z_H (not to be confused with the velocity of a random
 301 walker) is:

302
$$V_H(t) = \langle Z_H^2(t) \rangle = N_H^2 \int_{\mathbb{R}} (G_{1,H}(t-s)_+ - G_{1,H}(-s)_+)^2 ds \quad (22)$$

303 Equivalently, with an obvious change of change of variable:

304
$$V_H(t) = N_H^2 \int_0^{\infty} (G_{1,H}(s+t) - G_{1,H}(s))^2 ds + N_H^2 \int_0^t G_{1,H}(s)^2 ds \quad (23)$$

305 so that $V_H(0) = 0$. Z_H will converge in a root mean square sense if V_H converges. If

306 $G_{1,H}$ is a power law at large scales: $G_{1,H} \propto t^{H_l}; \quad t \gg 1$ then $H_l < 1/2$ is required for



307 convergence. Similarly, if at small scales $G_{1,H} \propto t^{H_h}$; $t \ll 1$, then convergence of
 308 V_H requires $H_h > -1/2$. We see that for fBm (eq. 13), $H_l = H_h = H$ so that this
 309 restriction implies $-1/2 < H < 1/2$ which is equivalent to the usual range $0 < H_B < 1$
 310 with $H_B = H + 1/2$. Similarly, for fRm, using $G^{(fRn)}_{1,H}(t)$, we have $H_h = H$, (eq. 15) and
 311 $H_l = -H$, (eq. 17) so that fRm converges for $H > -1/2$, i.e. over the entire range $0 < H <$
 312 2 discussed in this paper. Since the small scale limit of fRm is fBm, we see that
 313 range $0 < H < 2$ overlaps with the range of fBm and extends it at large H .

314 From eq. 19 we can consider the statistics of the increments:

$$\begin{aligned}
 Z_H(t) - Z_H(u) &= N_H \int_{\mathbb{R}} (G_{1,H}(t-s)_+ - G_{1,H}(u-s)_+) \gamma(s) ds \\
 &= N_H \int_{\mathbb{R}} (G_{1,H}(t-u-s')_+ - G_{1,H}(-s')_+) \gamma(s') ds'; \quad s' = s - u
 \end{aligned}
 \tag{24}$$

316 where we have used the fact that $\gamma(s') \stackrel{d}{=} \gamma(s)$ where $\stackrel{d}{=}$ means equality in a
 317 probability sense. This shows that:

$$Z_H(t) - Z_H(u) \stackrel{d}{=} Z_H(t-u) - Z_H(0) = Z_H(t-u)
 \tag{25}$$

319 so that the increments $Z_H(t)$ are stationary. From this, we obtain the variance of the
 320 increments $\Delta Z_H(\Delta t) = Z_H(t) - Z_H(t-\Delta t)$:

$$\langle \Delta Z_H(\Delta t)^2 \rangle = V_H(\Delta t); \quad \Delta t = t - u
 \tag{26}$$

322 Since $Z_H(t)$ is a mean zero Gaussian process, its statistics are determined by
 323 the covariance function:

$$C_H(t, u) = \langle Z_H(t) Z_H(u) \rangle = \frac{1}{2} (V_H(t) + V_H(u) - V_H(t-u))
 \tag{27}$$

325 The noises are the derivatives of the motions and as we mentioned, depending on H ,
 326 we only expect their finite integrals to converge. Let us therefore define the
 327 resolution τ noise $Y_{H,\tau}$ corresponding to the mean increments of the motions:

$$Y_{H,\tau}(t) = \frac{Z_H(t) - Z_H(t-\tau)}{\tau}
 \tag{28}$$

329 The noise, $Y_H(t)$ can now be obtained as the limit $\tau \rightarrow 0$:

$$Y_H(t) = \frac{dZ_H(t)}{dt}
 \tag{29}$$

331 Applying eq. 26, we obtain the variance:

$$\langle Y_{H,\tau}(t)^2 \rangle = \langle Y_{H,\tau}^2 \rangle = \tau^{-2} V_H(\tau)
 \tag{30}$$

332



333 since $\langle Y_{H,t}(0) \rangle = 0$, $Y_{H,\tau}(t)$ could be considered as the anomaly fluctuation of Y_H , so

334 that $\tau^{-2}V_H(\tau)$ is the anomaly variance at resolution τ .

335 From the covariance of Z_H (eq. 27) we obtain the correlation function:

$$R_{H,\tau}(\Delta t) = \langle Y_{H,\tau}(t)Y_{H,\tau}(t-\Delta t) \rangle = \tau^{-2} \langle (Z_H(t) - Z_H(t-\tau))(Z_H(t-\Delta t) - Z_H(t-\Delta t-\tau)) \rangle$$

$$= \tau^{-2} \frac{1}{2} (V_H(\Delta t - \tau) + V_H(\Delta t + \tau) - 2V_H(\Delta t)) \quad \Delta t \geq \tau$$

336

$$337 \quad R_{H,\tau}(0) = \langle Y_{H,\tau}(t)^2 \rangle = \tau^{-2}V_H(\tau); \quad \Delta t = 0 \quad (31)$$

338 Alternatively, taking time in units of the resolution $\lambda = \Delta t/\tau$:

$$R_{H,\tau}(\lambda\tau) = \langle Y_{H,\tau}(t)Y_{H,\tau}(t-\lambda\tau) \rangle = \tau^{-2} \langle (Z_H(t) - Z_H(t-\tau))(Z_H(t-\lambda\tau) - Z_H(t-\lambda\tau-\tau)) \rangle$$

$$= \tau^{-2} \frac{1}{2} (V_H((\lambda-1)\tau) + V_H((\lambda+1)\tau) - 2V_H(\lambda\tau)) \quad \lambda \geq 1$$

339

$$340 \quad R_{H,\tau}(0) = \langle Y_{H,\tau}(t)^2 \rangle = \tau^{-2}V_H(\tau); \quad \lambda = 0 \quad (32)$$

341 $R_{H,\tau}$ can be conveniently written in terms of centred finite differences:

$$342 \quad R_{H,\tau}(\lambda\tau) = \frac{1}{2} \Delta_\tau^2 V_H(\lambda\tau) \approx \frac{1}{2} V_H''(\Delta t); \quad \Delta_\tau f(t) = \frac{f(t+\tau/2) - f(t-\tau/2)}{\tau} \quad (33)$$

343 The finite difference formula is valid for $\Delta t \geq \tau$. For finite τ , it allows us to obtain the
 344 correlation behaviour by replacing the second difference by a second derivative, an
 345 approximation is very good except when Δt is close to τ .

346 Taking the limit $\tau \rightarrow 0$ in eq. 33 to obtain the second derivative of V_H , and after
 347 some manipulations, we obtain the following simple formula for the limiting
 348 function $R_H(\Delta t)$:

$$349 \quad R_H(\Delta t) = \frac{1}{2} \frac{d^2 V_H(\Delta t)}{d\Delta t^2} = \int_0^\infty G_{0,H}(s+\Delta t)G_{0,H}(s)ds; \quad G_{0,H} = \frac{dG_{1,H}}{ds} \quad (34)$$

350 If the integral for V_H converges, this integral for $R_H(\Delta t)$ will also converges except
 351 possibly at $\Delta t = 0$ (in the examples below, when $H \leq 1/2$).

352 Eq. 34 shows that R_H is the correlation function of the noise:

$$353 \quad Y_H(t) = \int_{-\infty}^t G_{0,H}(t-s)\gamma(s)ds \quad (35)$$

354 This result could have been derived formally from:

$$Y_H(t) = Z_H'(t) = \frac{dZ_H(t)}{dt} = \frac{d}{dt} \int_{-\infty}^t G_{1,H}(t-s)\gamma(s)ds;$$

$$= \int_{-\infty}^t G_{0,H}(t-s)\gamma(s)ds \quad (36)$$

355



356 but our derivation explicitly handles the convergence issues.

357 A useful statistical characterization of the processes is by the statistics of its
 358 Haar fluctuations over an interval Δt . For an interval Δt , Haar fluctuations are the
 359 differences between the averages of the first and second halves of an interval. For
 360 the noise Y_H , the Haar fluctuation is:

$$\Delta Y_H(\Delta t)_{Haar} = \frac{2}{\Delta t} \int_{t-\Delta t/2}^t Y_H(s) ds - \frac{2}{\Delta t} \int_{t-\Delta t}^{t-\Delta t/2} Y_H(s) ds \quad (37)$$

362 In terms of $Z_H(t)$:

$$\Delta Y_H(\Delta t)_{Haar} = \frac{2}{\Delta t} (Z_H(t) - 2Z_H(t - \Delta t/2) + Z_H(t - \Delta t)) \quad (38)$$

364 Therefore:

$$\begin{aligned} \langle \Delta Y_H(\Delta t)_{Haar}^2 \rangle &= \left(\frac{2}{\Delta t} \right)^2 \left(2 \langle \Delta Z_H(\Delta t/2)^2 \rangle - 2 \langle Y_{H,\Delta t/2}(t) Y_{H,\Delta t/2}(t - \Delta t/2) \rangle \right) \\ &= \left(\frac{2}{\Delta t} \right)^2 (4V_H(\Delta t/2) - V_H(\Delta t)) \end{aligned} \quad (39)$$

365 This formula will be useful below.

367 3 Application to fBm, fGn, fRm, fRn:

368 3.1 fBM, fGn:

369 The above derivations were for noises and motions derived from differential
 370 operators whose impulse and step Green's functions had convergent $V_H(t)$. Before
 371 applying them to fRn, fRm, we illustrate this by applying them first to fBm and fGn.

372 The fBm results are obtained by using the fGn step Green's function (eq. 13) in
 373 eq. 23 to obtain:

$$V_H^{(fBm)}(t) = N_H^2 \left(-\frac{2 \sin(\pi H) \Gamma(-1-2H)}{\pi} \right) t^{2H+1}; \quad -\frac{1}{2} \leq H < \frac{1}{2} \quad (40)$$

375 The standard normalization and parametrisation is:

$$\begin{aligned} N_H = K_H &= \left(-\frac{\pi}{2 \sin(\pi H) \Gamma(-1-2H)} \right)^{1/2} \\ &= \left(\frac{\pi (H_B + 1/2)}{2 \cos(\pi H_B) \Gamma(-2H_B)} \right)^{1/2}; \quad H_B = H + \frac{1}{2}; \quad 0 \leq H_B < 1 \end{aligned} \quad (41)$$

377 This normalization turns out to be convenient for both fBm and fRm so that we use
 378 it below to obtain:

$$V_{H_B}^{(fBm)}(t) = t^{2H+1} = t^{2H_B}; \quad 0 \leq H_B < 1 \quad (42)$$

380 so that:



381 $\left\langle \Delta B_H(\Delta t)^2 \right\rangle^{1/2} = \Delta t^{H_B}; \quad \Delta B_H(\Delta t) = B_H(t) - B_H(t - \Delta t)$ (43)

382 so – as mentioned earlier - H_B is the fluctuation exponent for fBm.

383 We can now calculate the correlation function relevant for the fGn statistics.

384 With the normalization $N_H = K_H$:

$$R_{H,\tau}^{(fGn)}(\lambda\tau) = \frac{1}{2} \tau^{2H-1} \left((\lambda+1)^{2H+1} + (\lambda-1)^{2H+1} - 2\lambda^{2H+1} \right); \quad \lambda \geq 1; \quad -\frac{1}{2} < H < \frac{1}{2}$$

385 $R_{H,\tau}^{(fGn)}(0) = \tau^{2H-1}$

386 $R_{H_B,\tau}^{(fGn)}(\lambda\tau) \approx H(2H+1)(\lambda\tau)^{2H-1} = H_B(2H_B-1)(\lambda\tau)^{2(H_B-1)}; \quad -\frac{1}{2} < H < \frac{1}{2}$ (44)
 $\lambda \gg 1$

387 the bottom line approximations are valid for large scale ratio λ . We note the
 388 difference in sign $H_B > 1/2$ (“persistence”), $H_B < 1/2$ (“antipersistence”). When $H_B =$
 389 $1/2$, the noise corresponds to usual Brownian motion, it is uncorrelated.

390 **3.2 fRm, fRn**

391 There are various cases to consider, appendix B gives some of the mathematical
 392 details including a small t series expansions for $0 < H < 3/2$; the leading terms are:

393 $V_H^{(fRm)}(t) = t^{1+2H} + O(t^{1+3H}); \quad N_H = K_H \quad 0 < H < 1/2$ (45)

394 $V_H^{(fRm)}(t) = t^2 - \frac{2\Gamma(-1-2H)\sin(\pi H)}{\pi C_H^2} t^{1+2H} + O(t^{1+3H}); \quad N_H = C_H^{-1}; \quad 1/2 < H < 3/2$

395 $V_H^{(fRm)}(t) = t^2 - \frac{t^4}{12C_H^2} \int_0^\infty G_{0,H}^{(fRm)}(s)^2 ds + O(t^{2H+1}); \quad 3/2 < H < 2$

396 $C_H^2 = \int_0^\infty G_{0,H}^{(fRm)}(s)^2 ds$

397

398 All for $t < 1$. The change in normalization for $H > 1/2$ is necessary since $K_H^2 < 0$ for
 399 this range. Similarly, the $H > 1/2$ normalization cannot be used for $H < 1/2$ since C_H
 400 diverges for $H < 1/2$. See fig. 2 for plots of $V^{(fRm)}_H(t)$. Note that the small t^2
 401 behaviour for $H > 1/2$ corresponds to fRm increments

402 $\left\langle \Delta Q_H^2(\Delta t) \right\rangle^{1/2} = \left(V_H^{(fRm)}(\Delta t) \right)^{1/2} \approx \Delta t$ i.e. to a smooth process, differentiable of order 1;

403 see section 3.4.

404 For large t , we have:

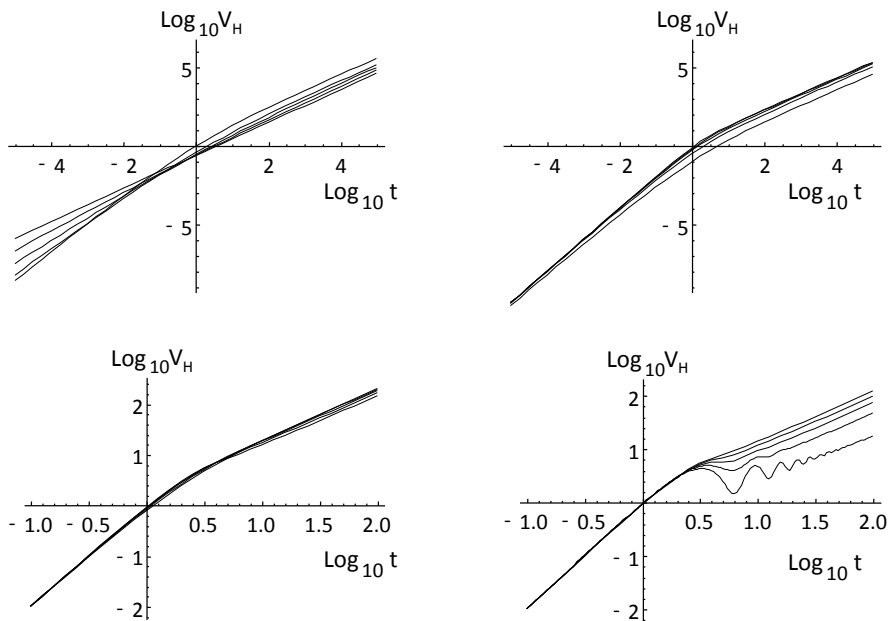


405
$$V_H^{(fRm)}(t) = N_H^2 \left[t - \frac{2t^{1-H}}{\Gamma(2-H)} + a_H + O(t^{1-2H}) \right]; \quad H < 1$$

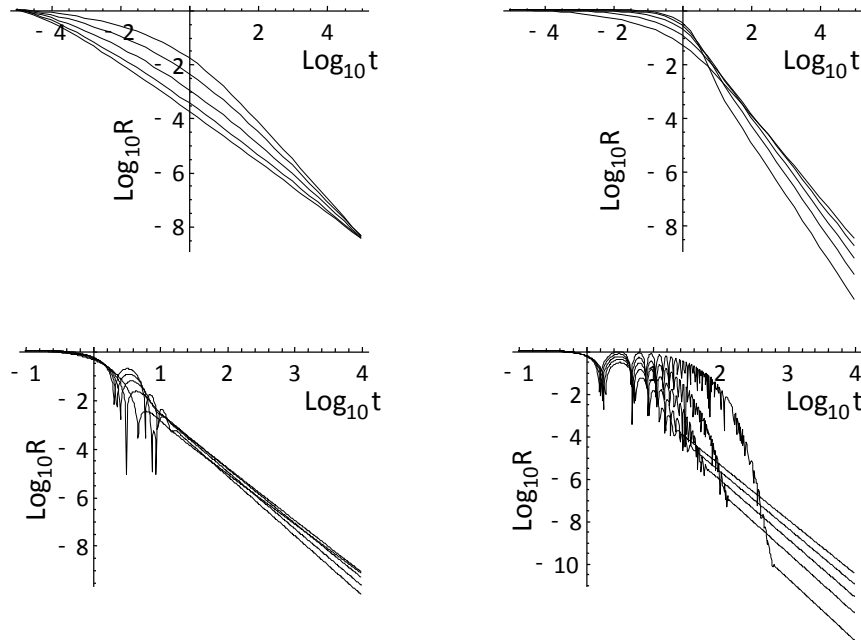
406
$$V_H^{(fRm)}(t) = N_H^2 \left[t + a_H - \frac{2t^{1-H}}{\Gamma(2-H)} + O(t^{1-2H}) \right]; \quad H > 1$$

(46)

407 where a_H is a constant, the above is valid for $t \gg 1$. Since $\langle \Delta Q_H(\Delta t)^2 \rangle = V_H(\Delta t)$, the
 408 corrections imply that at large scales $\langle \Delta Q_H(\Delta t)^2 \rangle^{1/2} < \Delta t^{1/2}$ so that the fRm process
 409 Q_H appears to be anti-persistent at large scales.



410 Fig. 2: The V_H functions for the various ranges of H for fRm (these characterize the variance
 411 of fRm). The plots from left to right, top to bottom are for the ranges $0 < H < 1/2$, $1/2 < H <$
 412 1 , $1 < H < 3/2$, $3/2 < H < 2$. Within each plot, the lines are for H increasing in units of $1/10$
 413 starting at a value $1/20$ above the plot minimum (ex. for the upper left, the lines are for $H =$
 414 $1/20, 3/10, 5/20, 7/20, 9/20$). For all H 's the large t behaviour is linear (slope = one,
 415 although note the oscillations for $3/2 < H < 2$). For small t , the slopes are $1+2H$ ($0 < H \leq 1/2$)
 416 and 2 ($1/2 \leq H < 2$).
 417



418
 419
 420 Fig. 3: The correlation functions R_H for fRn corresponding to the V_H function in fig. 2 $0 < H <$
 421 $1/2$ (upper left), $1/2 < H < 1$ (upper right), $1 < H < 3/2$ lower left, $3/2 < H < 2$ lower right.
 422 In each plot, the curves correspond to H increasing from bottom to top in units of $1/10$
 423 starting from $1/20$ (upper left) to $39/20$ (bottom right). For $H < 1/2$, the $R_{H,\tau}$ are shown
 424 with $\tau = 10^{-5}$; they were normalized to the value at resolution $\tau = 10^{-5}$. For $H > 1/2$, the
 425 curves are normalized with $N_H = 1/C_H$; for $H < 1/2$, they were normalized to the value at
 426 resolution $\tau = 10^{-5}$. In all cases, the large t slope is $-1-H$.
 427

428 The formulae for R_H can be obtained by differentiating the above results for V_H
 429 twice (eqs. 45, 46), see appendix B for details and Padé approximants):

430
$$R_H^{(fRn)}(t) = H(1+2H)t^{-1+2H} + O(t^{-1+3H}); \quad t \ll 1; \quad 0 < H < 1/2$$

431
$$R_H^{(fRn)}(t) = 1 - \frac{\Gamma(1-2H)\sin(\pi H)}{\pi C_H^2} t^{-1+2H} + O(t^{-1+3H}); \quad t \ll 1; \quad 1/2 < H < 3/2$$

432
$$R_H^{(fRn)}(t) = 1 - \frac{t^2}{2C_H^2} \int_0^\infty G'_{0,H}(s)^2 ds + O(t^{-1+2H}) \dots; \quad t \ll 1; \quad 3/2 < H < 2 \quad (47)$$

433 (when $0 < H < 1/2$, for $t \approx \tau$ we must use the resolution τ fGn formula, eq. 44, top).
 434 For large t :



435
 436

$$437 \quad R_H^{(fRn)}(t) = -\frac{N_H^2}{\Gamma(-H)} t^{-1-H} + O(t^{-1-2H}): \quad 0 < H < 2 \quad ; t \gg 1 \quad (48)$$

438 Note that for $0 < H < 1$, $\Gamma(-H) < 0$ so that $R > 0$ over this range (fig. 3). Also, when $H < 1/2$,
 439 we see (eq. 47) that $R_H(t)$ diverges in the small scale limit so that we must use $R_{H,\tau}(t)$ and
 440 the corresponding small t formula above is only valid for $1 \gg t \gg \tau$. When $t \approx \tau$, the exact
 441 formula (eq. 31) must be used. Formulae 45, 47 show that there are three qualitatively
 442 different regimes: $0 < H < 1/2$, $1/2 < H < 3/2$, $3/2 < H < 2$; this is in contrast with the
 443 deterministic relaxation and oscillation regimes ($0 < H < 1$ and $1 < H < 2$). We return to
 444 this in section 3.4.

445 Now that we have worked out the behaviour of the correlation function, we can
 446 comment on the issue of the memory of the process. Starting in turbulence, there is the
 447 notion of “integral scale” that is conventionally defined as the long time integral of the
 448 correlation function. When the integral scale diverges, the process is conventionally
 449 termed a “long memory process”. With this definition, if the long time exponent of R_H is
 450 > -1 , then the process has a long memory. Eq. 48 shows that the long time exponent is
 451 $-1-H$ so that for all H considered here, the integral scale converges. However, it is of the
 452 order of the relaxation time which may be much larger. For example, eq. 47 shows that
 453 when $H < 1/2$, the effective exponent $2H - 1$ implies (in the absence of a cut-off), a
 454 divergence at long times, so that fRn mimics a long memory process.

455 3.3 Haar fluctuations

456 Using eq. 39 we can determine the behaviour of the RMS Haar fluctuations.

457 Applying this equation to fGn we obtain $\left\langle \Delta F_H(\Delta t)_{Haar}^2 \right\rangle^{1/2} \propto \Delta t^{H_{Haar}}$ with $H_{Haar} = H -$

458 $1/2$ (the subscript “Haar” indicates that this is not a difference/increment
 459 fluctuation but rather a Haar fluctuation). For the motion, the Haar exponent is

460 equal to the exponents of the increments (eq. 43) so that $\left\langle \Delta B_H(\Delta t)_{Haar}^2 \right\rangle^{1/2} \propto \Delta t^{H_{Haar}}$

461 with $H_{Haar} = H_B = H + 1/2$ (both results were obtained in [Lovejoy *et al.*, 2015]).
 462 Therefore, from an empirical viewpoint if we have a scaling Gaussian process and
 463 when $-1/2 < H_{Haar} < 0$, it has the scaling of an fGn and when $0 < H_{Haar} < 1/2$, it scales
 464 as an fBm.

465 Using eq. 39, we can determine the Haar fluctuations for fRn $\left\langle \Delta U_H(\Delta t)_{Haar}^2 \right\rangle^{1/2}$.

466 With the small and large t approximations for $V_H(t)$, we can obtain the small and
 467 large Δt behaviour of the Haar fluctuations. Therefore, the leading terms for small
 468 Δt are:



469
$$\left\langle \Delta U_H (\Delta t)_{Haar}^2 \right\rangle^{1/2} = \Delta t^{H_{Haar}} \quad \begin{matrix} H_{Haar} = H - 1/2; & 0 < H < 3/2 \\ H_{Haar} = 1; & 3/2 < H < 2 \end{matrix}; \quad \Delta t \ll 1 \quad (49)$$

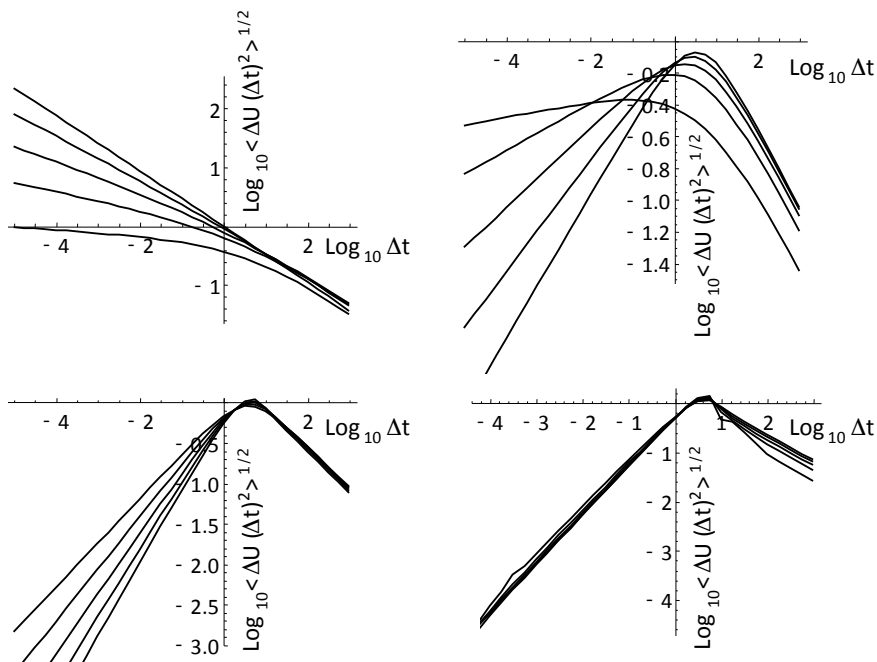
470 where the $\Delta t^{H-1/2}$ behaviour comes from terms in $V_H \approx t^{1+2H}$ and the Δt behaviour
 471 from the $V_H \approx t^4$ terms that arise when $H > 3/2$. Note (eq. 39) that $\left\langle \Delta U_H (\Delta t)_{Haar}^2 \right\rangle^{1/2}$
 472 depends on $4V_H(\Delta t/2) - V_H(\Delta t)$ so that quadratic terms in $V_H(t)$ cancel.

473 As H increases past the critical value $H = 1/2$, the sign of H_{Haar} changes so that
 474 when $1/2 < H < 3/2$, we have $0 < H_{Haar} < 1$ so that over this range, the small Δt
 475 behaviour mimics that of fBm rather than fGn (discussed in the next section).

476 For large Δt , the corresponding formula is:

477
$$\left\langle \Delta U_{Haar}^2 (\Delta t)^2 \right\rangle^{1/2} \propto \Delta t^{-1/2}; \quad \Delta t \gg 1; \quad 0 < H < 2 \quad (50)$$

478 This white noise scaling is due to the leading behavior $V_H(t) \approx t$ over the full range of
 479 H (eq. 47), see fig. 4a.



480 Fig. 4a: The RMS Haar fluctuation plots for the fRn process for $0 < H < 1/2$ (upper left), $1/2 < H$
 481 < 1 (upper right), $1 < H < 3/2$ (lower left), $3/2 < H < 2$ (lower right). The individual curves
 482 correspond to those of fig. 2, 3. The small Δt slopes follow the theoretical values $H - 1/2$ up to
 483



484 $H = 3/2$ (slope= 1); for larger H , the small t slopes all = 1. Also, at large t due to dominant V
 485 $\approx t$ terms, in all cases we obtain slopes $t^{-1/2}$.
 486

487 **3.4 fBm, fRm or fGn?**

488 Our analysis has shown that there are three regimes with qualitatively
 489 different small scale behaviour, let us compare them in more detail. The easiest
 490 way to compare the different regimes is to consider their increments. Since fRn is
 491 stationary, we can use:

492
$$\langle \Delta U_H(\Delta t)^2 \rangle = \langle (U_H(t) - U_H(t - \Delta t))^2 \rangle = 2(R_H^{(fRn)}(0) - R_H^{(fRn)}(\Delta t)) \quad (51)$$

493 Over the various ranges for small Δt , we have:

494
$$\begin{aligned} \langle \Delta U_{H,\tau}(\Delta t)^2 \rangle &\approx 2\tau^{-1+2H} - 2H(2H+1)\Delta t^{-1+2H}; & \Delta t \gg \tau; & \quad 0 < H < 1/2 \\ \langle \Delta U_H(\Delta t)^2 \rangle &\approx \Delta t^{-1+2H}; & & \quad 1/2 < H < 3/2 \\ \langle \Delta U_H(\Delta t)^2 \rangle &\approx \Delta t^2; & & \quad 3/2 < H < 2 \end{aligned} \quad (52)$$

495 We see that in the small H range, the increments are dominated by the
 496 resolution τ , the process is a noise that does not converge point-wise, hence the τ
 497 dependence. In the middle ($1/2 < H < 3/2$) regime, the process is point-wise
 498 convergent (take the limit $\tau \rightarrow 0$) although it cannot be differentiated by any integer
 499 order. Finally, the largest H regime, the process is smoother:

500
$$\lim_{\Delta t \rightarrow 0} \langle (\Delta U_H(\Delta t) / \Delta t)^2 \rangle = 1$$
, so that it is almost surely differentiable of order 1. Since

501 the fRm are simply integrals of fRn, their orders of differentiability are simply
 502 augmented by one.

503 Considering the first two ranges i.e. $0 < H < 3/2$, we therefore have several
 504 processes with the same small scale statistics and this may lead to difficulties in
 505 interpreting empirical data that cover ranges of time scales smaller than the
 506 relaxation time. For example, we already saw that over the range $0 < H < 1/2$ that
 507 at small scales we could not distinguish fRn from the corresponding fGn; they both
 508 have anomalies (averages after the removal of the mean) or Haar fluctuations that
 509 decrease with time scale (exponent $H - 1/2$, eq. 49). This similitude was not
 510 surprising since they both were generated by Green's functions with the same high
 511 frequency term. From an empirical point of view, it might be impossible to
 512 distinguish the two since over scales much smaller than the relaxation time, their
 513 statistics can be very close.

514 The problem is compounded when we turn to increments or fluctuations that
 515 increase with scale. To see this, note that in the middle range ($1/2 < H < 3/2$), the
 516 exponent $-1 + 2H$ spans the range 0 to 2. This is the same range spanned by fRm (Q_H)
 517 with $0 < H < 1/2$:



518 $\langle \Delta Q_H(\Delta t)^2 \rangle = V_H^{(fRm)}(\Delta t) \propto \Delta t^{1+2H}; \quad \Delta t \ll 1; \quad 0 < H < 1/2$
 519 and with fBm (B_H) over the same H range (but for all Δt):

520 $\langle \Delta B_H(\Delta t)^2 \rangle = V_H^{(fBm)}(\Delta t) = \Delta t^{1+2H}; \quad 0 < H < 1/2$
 521 (54)

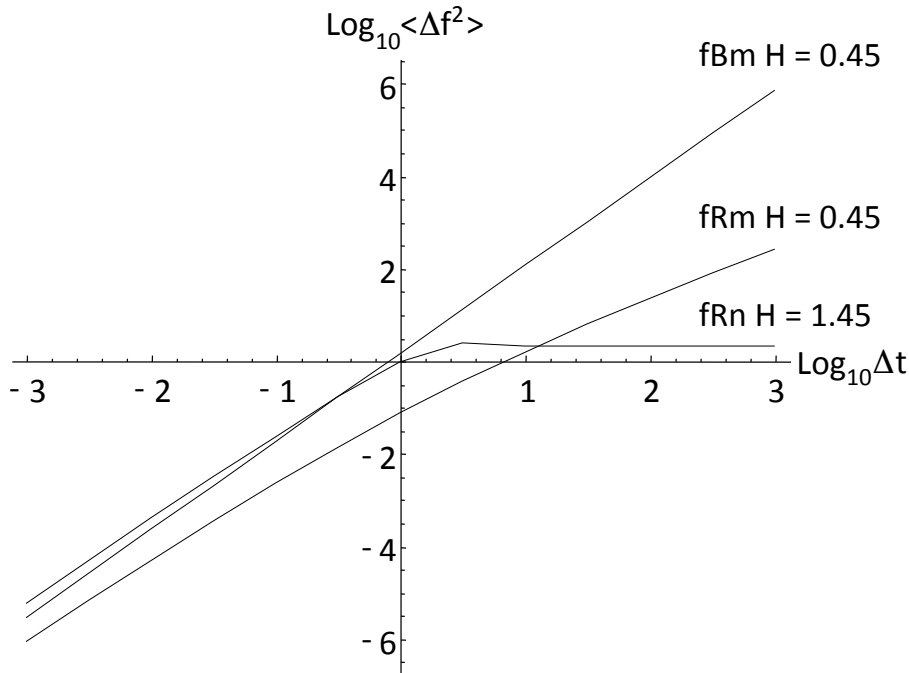
521 If we use the usual fBm exponent $H_B = H + 1/2$, then, over the range $0 < H < 1/2$ we
 522 may not only compare fBm with fRm with the same H_B , but also with an fRn process
 523 with an H larger by unity, i.e. with $H_B = H - 1/2$ in the range $1/2 < H < 3/2$. In this
 524 case, we have:
 525

526 $\langle \Delta U_H(\Delta t)^2 \rangle \propto \Delta t^{2H_B}; \quad \Delta t \ll 1; \quad 0 < H_B < 1$
 $\propto 2(1 - a\Delta t^{-H_B-3/2}); \quad \Delta t \gg 1$
 (55)

527 $\langle \Delta Q_H(\Delta t)^2 \rangle \propto \Delta t^{2H_B}; \quad \Delta t \ll 1; \quad 1/2 < H_B < 1$
 $\propto \Delta t - b\Delta t^{3/2-H_B}; \quad \Delta t \gg 1$

528 $\langle \Delta B_H(\Delta t)^2 \rangle = \Delta t^{2H_B}; \quad 0 < H_B < 1$
 529

530 where a, b are constants (section 3.2). Over the entire range $0 < H_B < 1$, we see that
 531 the only difference between fBm, and fRn is their different large scale behaviours.
 532 Therefore, if we found a process that over a finite range was scaling with exponent
 533 $1/2 < H_B < 1$, then over that range, we could not tell the difference between fRn, fRm,
 534 fBm, see fig. 4b for an example with $H_B = 0.95$.
 535



536
 537 Fig. 4b: A comparison of fRn with $H = 1.45$, fRm with $H = 0.45$ and fBm with $H = 0.45$. For
 538 small Δt , they all have RMS increments with exponent $H_B = 0.95$ and can only be
 539 distinguished by their behaviours at Δt larger than the relaxation time ($\log_{10} \Delta t = 0$ in this
 540 plot).

541 **3.5 Spectra:**

542 Since $Y_H(t)$ is stationary process, its spectrum is the Fourier transform of the
 543 correlation function $R_H(t)$ (the Wiener-Khintchin theorem). However, it is easier to
 544 determine it directly from the fractional relaxation equation using the fact that the
 545 Fourier transform (F.T., indicated by the tilde) of the Weyl fractional derivative is
 546 simply $F.T. \left[{}_{-\infty} D_t^H Y_H \right] = (-i\omega)^H \tilde{Y}_H(\omega)$ (e.g. [Podlubny, 1999]). Therefore take the F.T. of
 547 eq. 4 (the fRn), to obtain:

$$548 \left((-i\omega)^H + 1 \right) \tilde{U}_H = \tilde{\gamma} \tag{56}$$

549 so that the spectrum of Y is:



$$\begin{aligned}
 E_U(\omega) &= \left\langle \left| \widetilde{U}_H(\omega) \right|^2 \right\rangle = \frac{\left\langle \left| \widetilde{\gamma}(\omega) \right|^2 \right\rangle}{\left(1 + (-i\omega)^H\right)\left(1 + (i\omega)^H\right)} = \frac{1}{\left(1 + (-i\omega)^H\right)\left(1 + (i\omega)^H\right)} \\
 &= \left(1 + 2\cos\left(\frac{\pi H}{2}\right)\omega^H + \omega^{2H}\right)^{-1}
 \end{aligned}
 \tag{57}$$

The asymptotic high and low frequency behaviours are therefore,

$$\begin{aligned}
 E_U(\omega) &= \begin{cases} \omega^{-2H} + O(\omega^{-3H}); & \omega \gg 1 \\ 1 - 2\cos\left(\frac{\pi H}{2}\right)\omega^H + O(\omega^{2H}) & \omega \ll 1 \end{cases}
 \end{aligned}
 \tag{58}$$

This corresponds to the scaling regimes determined by direct calculation above:

$$R_H(t) \propto \begin{cases} t^{-1+2H} + \dots & t \ll 1 \\ t^{-1-H} + \dots & t \gg 1 \end{cases}
 \tag{59}$$

Note that the usual (Orenstein-Uhlenbeck) result for $H = 1$ has no ω^H term, hence no t^{1-H} term; it has an exponential rather than power law decay at large t .

From the spectrum of U , we can easily determine the spectrum of the stationary Δt increments of the fRm process Q_H :

$$E_{\Delta Q}(\omega) = \left(\frac{2\sin\frac{\omega\Delta t}{2}}{\omega} \right)^2 E_U(\omega); \quad \Delta Q(\Delta t) = \int_{t-\Delta t}^t U(s) ds
 \tag{60}$$

3.6 Sample processes

It is instructive to view some samples of fRn, fRm processes. For this purpose, we can use the solution for fRn in the form of a convolution (eq. 35), and use numerical convolution algorithms. Simulations of fRn are best made by simulating the motions Q_H and then taking finite differences using: $Q_H = G_{1,H} * \gamma$ (* denotes a Weyl convolution). This allows us to use the nonsingular G_1 rather than the singular G_0 .

In order to clearly display the behaviours, recall that when $t \gg 1$, we showed that all the fRn converge to Gaussian white noises and the fRm to Brownian motions (albeit in a slow power law manner). At the other extreme, for $t \ll 1$, we obtain the fGn and fBm limits (when $0 < H < 1/2$) and their generalizations for $1/2 < H < 2$.

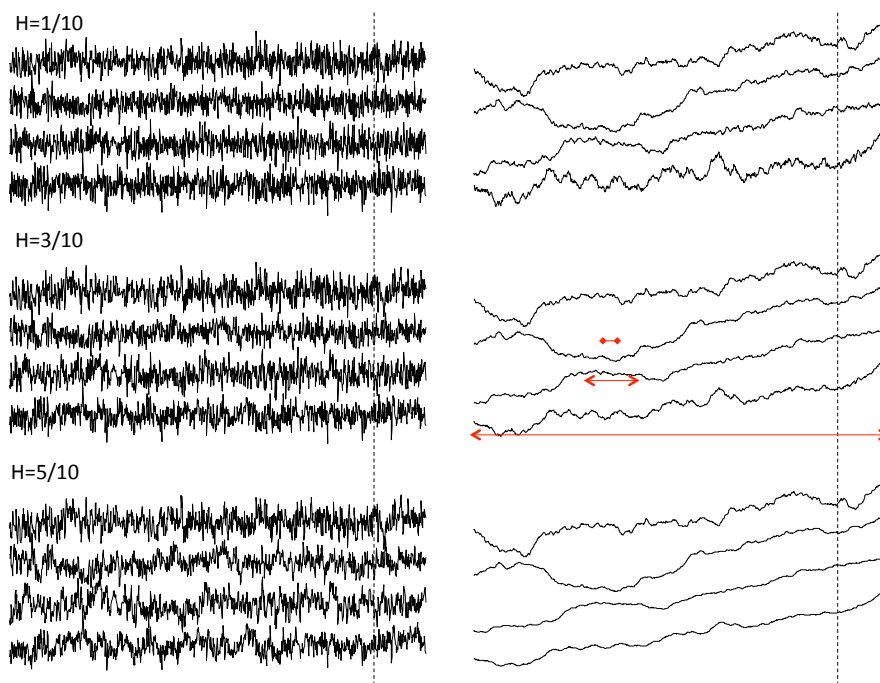
Fig. 5a shows three simulations, each of length 2^{19} , pixels, with each pixel corresponding to a temporal resolution of $\tau = 2^{-10}$. Each simulation uses the same random seed but they have H 's increasing from $H = 1/10$ (top set) to $H = 5/10$ (bottom set). The fRm at the right is from the running sum of the fRn at the left. Each series has been rescaled so that the range (maximum - minimum) is the same for each. Starting at the top line of each group, we show 2^{10} points of the original



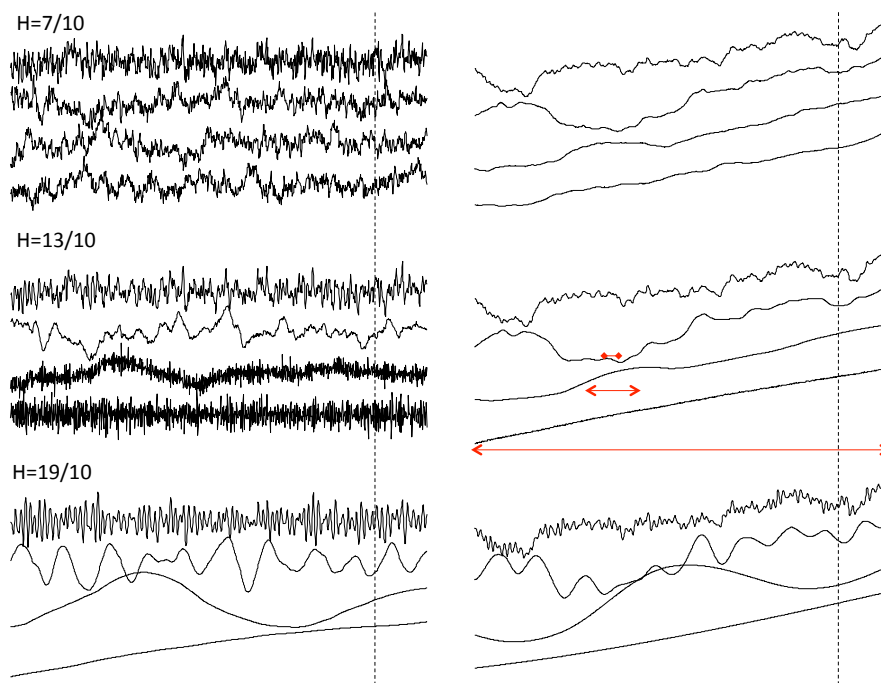
577 series degraded by a factor 2^9 . The second line shows a blow-up by a factor of 8 of
578 the part of the upper line to the right of the dashed vertical line. The line below is a
579 further blow up by factor of 8, until the bottom line shows $1/512$ part of the full
580 simulation, but at full resolution. The unit scale indicating the transition from small
581 to large is shown by the horizontal red line in the middle right figure. At the top
582 (degraded by a factor 2^9), the unit (relaxation) scale is 2 pixels so that the top line
583 degraded view of the simulation is nearly a white noise (left), (ordinary) Brownian
584 motion (right). In contrast, the bottom series is exactly of length unity so that it is
585 close to the fGn limit with the standard exponent $H_B = H + 1/2$.

586 Fig. 5b shows realizations constructed from the same random seed but for the
587 extended range $1/2 < H < 2$ (i.e. beyond the fGn range). Over this range, the top
588 (large scale, degraded resolution) series is close to a white noise (left) and Brownian
589 motion (right). For the bottom series, there is no equivalent fGn or fBm process, the
590 curves become smoother although the rescaling may hide this somewhat (see for
591 example the $H = 13/20$ set, the blow-up of the far right $1/8$ of the second series from
592 the top shown in the third line. For $1 < H < 2$, also note the oscillations with
593 wavelength of order unity, this is the fractional oscillation range.

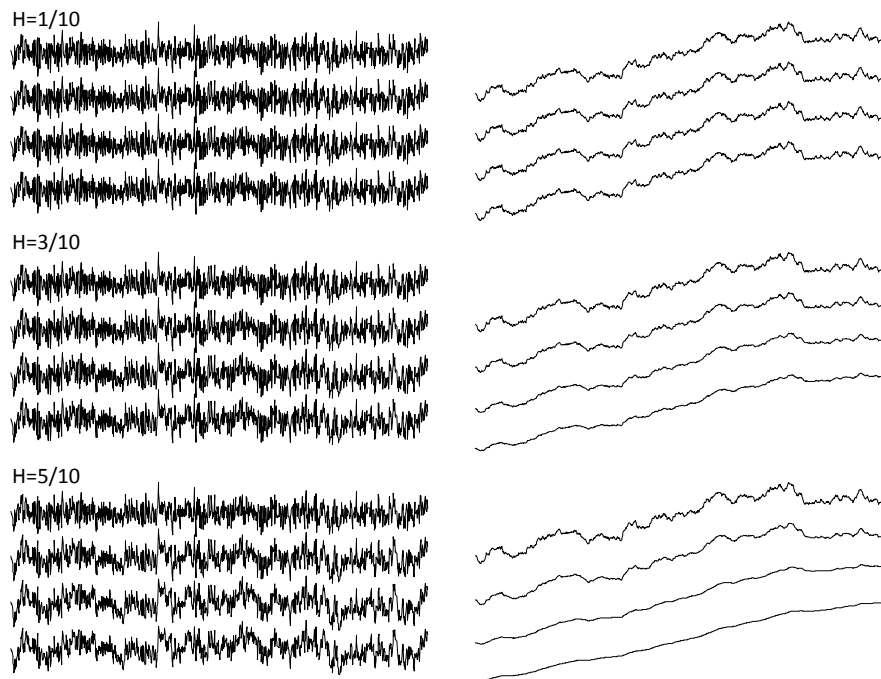
594 Fig. 6a shows simulations similar to fig. 5a (fRn on the left, fRm on the right)
595 except that instead of making a large simulation and then degrading and zooming,
596 all the simulations were of equal length (2^{10} points), but the relaxation scale was
597 changed from 2^{15} pixels (bottom) to 2^{10} , 2^5 and 1 pixel (top). Again the top is white
598 noise (left), Brownian motion (right), and the bottom is (nearly) fGn (left) and fBm
599 (right), fig. 6b shows the extensions to $1/2 < H < 2$.



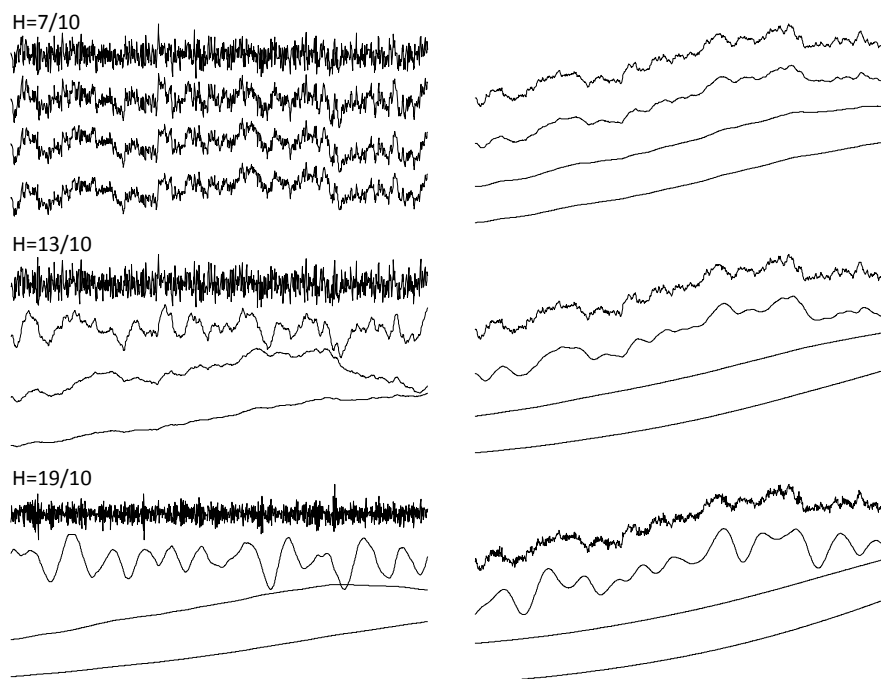
600
601 Fig. 5a: fRn and fRm simulations (left and right columns respectively) for $H = 1/10, 3/10,$
602 $5/10$ (top to bottom sets) i.e. the range that overlaps with fGn and fBm. There are three
603 simulations, each of length 2^{19} , each use the same random seed. The fRm at the right is from
604 the running sum of the fRn at the left. Starting at the top line of each group, we show 2^{10}
605 points of the originals series degraded by a factor 2^9 . The second line shows a blow-up by a
606 factor of 8 of the part of the upper line to the right of the dashed vertical line (note, each
607 series was rescaled so that its range between maximum and minimum was the same). The
608 line below each is a further blow up by factor of 8, until the bottom line shows $1/512$ part of
609 the full simulation, but at full resolution. The unit scale indicating the transition from small
610 to large is shown by the horizontal red line in the middle right figure. At the top (degraded
611 by a factor 2^9), the unit scale is 2 pixels (too small to be shown in red) so that the strongly
612 degraded view at the top of each simulation is nearly a white noise (left), or (ordinary)
613 Brownian motion (right). In contrast, the bottom series is exactly of length unity so that it is
614 close to the fGn limit with the standard exponent $H_B = H + 1/2$.
615



616
617 Fig. 5b: The same as fig. 5a but for $H = 7/10, 13/10$ and $19/10$ (top to bottom). Over this
618 range, the top (large scale, degraded resolution) series is close to a white noise (left) and
619 Brownian motion (right). For the bottom series, there is no equivalent fGn or fBm process,
620 the curves become smoother although the rescaling may hide this somewhat (see for
621 example the $H = 13/20$ set, the blow-up of the far right $1/8$ of the second series from the top
622 shown in the third line). Also note for the bottom two sets with $1 < H < 2$, the oscillations
623 that have wavelengths of order unity, this is the fractional oscillation range.
624



625
626 Fig. 6a: This set of simulations is similar to fig. 5a (fRn on the left, fRm on the right) except
627 that instead of making a large simulation and then degrading and zooming, all the
628 simulations were of equal length (2^{10} points), but the unit scale (the relaxation time) was
629 changed from 2^{15} pixels (bottom row of each set) to 2^{10} , 2^5 and 1 pixel (top). The top series
630 (of total length 2^{10} relaxation times) is (nearly) a white noise (left), and Brownian motion
631 (right), and the bottom is (spanning a range of scales from 2^{-15} to 2^{-5} relaxation times) is
632 (nearly) an fGn (left) and fBm (right). The total range of scales covered here ($2^{10} \times 2^{15}$) is
633 larger than in fig. 5a and allows one to more clearly distinguish the high and low frequency
634 regimes.
635



636
637 Fig. 6b: The same fig. 6a but for larger H values; see also fig. 5b.

638 4. Prediction

639 The initial value for Weyl fractional differential equations is effectively at
640 $t = -\infty$, so that it is not relevant at finite times. The prediction problem is thus to
641 use past data (say, for $t < 0$) in order to make the most skilful prediction of the
642 future noises and motions at $t > 0$. We are therefore dealing with a *past value* rather
643 than a usual *initial value* problem. The emphasis on past values is particularly
644 appropriate since in the fGn limit, the memory is so large that values of the series in
645 the distant past are important. Indeed, prediction with a finite length of past data
646 involves placing strong (mathematically singular) weights on the most ancient data
647 available (see [Gripenberg and Norros, 1996], [Del Rio Amador and Lovejoy, 2019]).

648 In general, there will be small scale divergences (for fRn, when $0 < H \leq 1/2$) so
649 that it is important to predict the finite resolution fRn: $Y_{H,\tau}(t)$. Using eq. 28 for
650 $Y_{H,\tau}(t)$, we have:



$$\begin{aligned}
 Y_{H,\tau}(t) &= \frac{1}{\tau} \left[\int_{-\infty}^t G_{1,H}(t-s)\gamma(s)ds - \int_{-\infty}^0 G_{1,H}(-s)\gamma(s)ds \right] - \\
 &\quad \frac{1}{\tau} \left[\int_{-\infty}^{t-\tau} G_{1,H}(t-\tau-s)\gamma(s)ds - \int_{-\infty}^0 G_{1,H}(-s)\gamma(s)ds \right] \\
 &= \frac{1}{\tau} \left[\int_{-\infty}^t G_{1,H}(t-s)\gamma(s)ds - \int_{-\infty}^{t-\tau} G_{1,H}(t-\tau-s)\gamma(s)ds \right]
 \end{aligned}
 \tag{61}$$

651

652 Defining the predictor for $t \geq 0$ (indicated by a circonflex):

$$\widehat{Y}_{\tau}(t) = \frac{1}{\tau} \left[\int_{-\infty}^0 G_{1,H}(t-s)\gamma(s)ds - \int_{-\infty}^0 G_{1,H}(t-\tau-s)\gamma(s)ds \right]
 \tag{62}$$

653

654 We see that the error $E_{\tau}(t)$ in the predictor is:

$$\begin{aligned}
 E_{\tau}(t) &= Y_{\tau}(t) - \widehat{Y}_{\tau}(t) = \tau^{-1} \left[\int_{-\infty}^t G_{1,H}(t-s)\gamma(s)ds - \int_{-\infty}^{t-\tau} G_{1,H}(t-\tau-s)\gamma(s)ds \right] \\
 &\quad - \tau^{-1} \left[\int_{-\infty}^0 G_{1,H}(t-s)\gamma(s)ds - \int_{-\infty}^0 G_{1,H}(t-\tau-s)\gamma(s)ds \right] \\
 &= \tau^{-1} \left[\int_0^t G_{1,H}(t-s)\gamma(s)ds - \int_0^{t-\tau} G_{1,H}(t-\tau-s)\gamma(s)ds \right]
 \end{aligned}
 \tag{63}$$

655

656 Eq. 63 shows that the error depends only on $\gamma(s)$ for $s > 0$ whereas the predictor (eq.
 657 62) only depends on $\gamma(s)$ so that for $s < 0$ they are orthogonal:

$$\langle E_{\tau}(t) \widehat{Y}_{\tau}(t) \rangle = 0
 \tag{64}$$

658

659 Hence, $\widehat{Y}_{\tau}(t)$ is the minimum square predictor which is the optimal predictor for
 660 Gaussian processes, (e.g. [Papoulis, 1965]). The prediction error variance is:

$$\langle E_{\tau}(t)^2 \rangle = \tau^{-2} \left[\int_0^{t-\tau} (G_{1,H}(t-s) - G_{1,H}(t-\tau-s))^2 ds + \int_{t-\tau}^t G_{1,H}(t-s)^2 ds \right]
 \tag{65}$$

661

662 or with a change of variables:

$$\langle E_{\tau}(t)^2 \rangle = \tau^{-2} N_H^{-2} V_H(\tau) - \tau^{-2} \left[\int_{t-\tau}^{\infty} (G_{1,H}(u+\tau) - G_{1,H}(u))^2 du \right]
 \tag{66}$$

663

664 where we have used $\langle Y_{\tau}^2 \rangle = \tau^{-2} N_H^{-2} V_H(\tau)$ (the unconditional variance).

665 Using the usual definition of forecast skill (also called the Minimum Square
 666 Skill Score or MSSS):



$$\begin{aligned}
 S_{k,\tau}(t) &= 1 - \frac{\langle E_\tau(t)^2 \rangle}{\langle E_\tau(\infty)^2 \rangle} = \frac{\langle E_\tau(t)^2 \rangle}{\tau^{-2} N_H^{-2} V_H(\tau)} = \frac{N_H^2 \int_{t-\tau}^{\infty} (G_{1,H}(u+\tau) - G_{1,H}(u))^2 du}{V_H(\tau)} \\
 &= \frac{\int_{t-\tau}^{\infty} (G_{1,H}(u+\tau) - G_{1,H}(u))^2 du}{\int_0^{\infty} (G_{1,H}(u+\tau) - G_{1,H}(u))^2 du + \int_0^{\tau} G_{1,H}(u)^2 du}
 \end{aligned} \tag{67}$$

667
 668 When $H < 1/2$ and $G_{1,H}(t) = G_{1,H}^{(fGn)}(t) = \frac{t^H}{\Gamma(1+H)}$, we can check that we obtain the fGn
 669 result:

$$\int_{t-\tau}^{\infty} (G_{1,H}(u+\tau) - G_{1,H}(u))^2 du \approx \frac{\tau^{1+2H}}{\Gamma(1+H)^2} \int_{\lambda-1}^{\infty} ((v+1)^H - v^H)^2 dv; \quad v = u/\tau; \quad \lambda = t/\tau \tag{68}$$

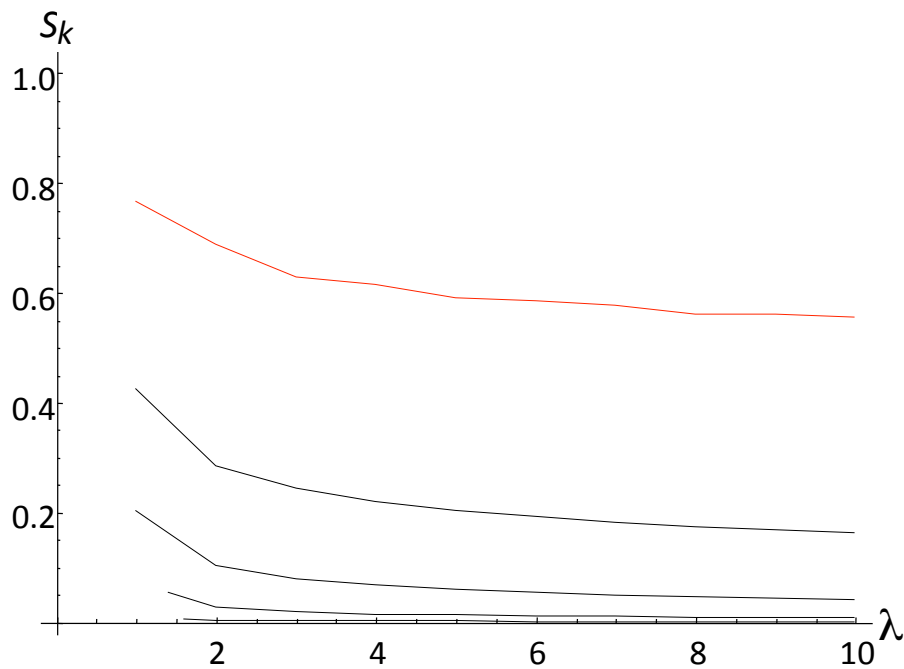
670
 671 [Lovejoy et al., 2015]. This can be expressed in terms of the function:

$$\xi_H(\lambda) = \int_0^{\lambda-1} ((u+1)^H - u^H)^2 du \tag{69}$$

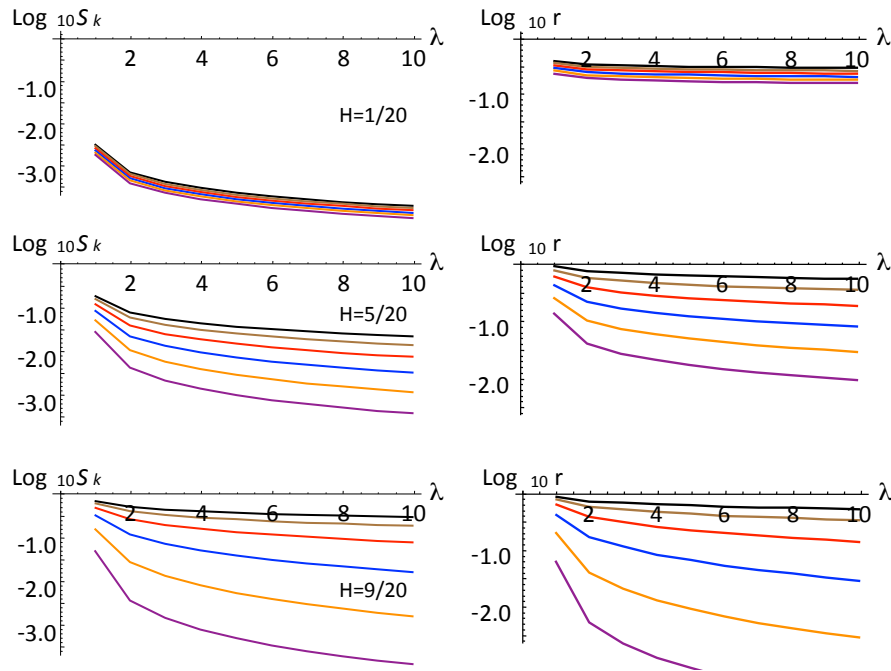
672
 673 So that the usual fGn result (independent of τ) is:

$$S_k = \frac{\xi_H(\infty) - \xi_H(\lambda)}{\xi_H(\infty) + \frac{1}{2H+1}} \tag{70}$$

674
 675 To survey the implications, let's start by showing the τ independent results for
 676 fGn, shown in fig. 7 which is a variant on a plot published in [Lovejoy et al., 2015].
 677 We see that when $H \approx 1/2$ ($H_B \approx 1$) that the skill is very high, indeed, in the limit
 678 $H \rightarrow 1/2$, we have perfect skill for fGn forecasts (this would of course require an
 679 infinite amount of past data to attain).
 680



681
682 Fig. 7: The prediction skill (S_k) for pure fGn processes for forecast horizons up to $\lambda =$
683 10 steps (ten times the resolution). This plot is non-dimensional, it is valid for time
684 steps of any duration. From bottom to top, the curves correspond to $H = 1/20, 3/10,$
685 $\dots 9/20$ (red, top).
686



687
 688 Fig. 8: The left column shows the skill (S_k) of fRn forecasts (as in fig. 7 for fGn) for
 689 fRn skill with $H = 1/20, 5/20, 9/20$ (top to bottom set); λ is the forecast horizon, the
 690 number of steps of resolution τ forecast into the future. Here the result depends on
 691 τ ; each curve is for different values increasing from 10^{-4} (top, black) to 10 (bottom,
 692 purple) increasing by factors of 10. The right hand column shows the ratio (r) of
 693 the fRn to corresponding fGn skill.

694
 695 Now consider the fRn skill. In this case, there is an extra parameter, the
 696 resolution of the data, τ . Figure 8 shows curves corresponding to fig. 7 for fRn with
 697 forecast horizons integer multiples (λ) of τ i.e. for times $t = \lambda\tau$ in the future, but with
 698 separate curves, one for each of five τ values increasing from 10^{-4} to 10 by factors of
 699 ten. When τ is small, the results should be close to those of fGn, i.e. with potentially
 700 high skill, and in all cases, the skill is expected to vanish quite rapidly for $\tau > 1$ since in
 701 this limit, fRn becomes an (unpredictable) white noise (although there are scaling
 702 corrections to this).

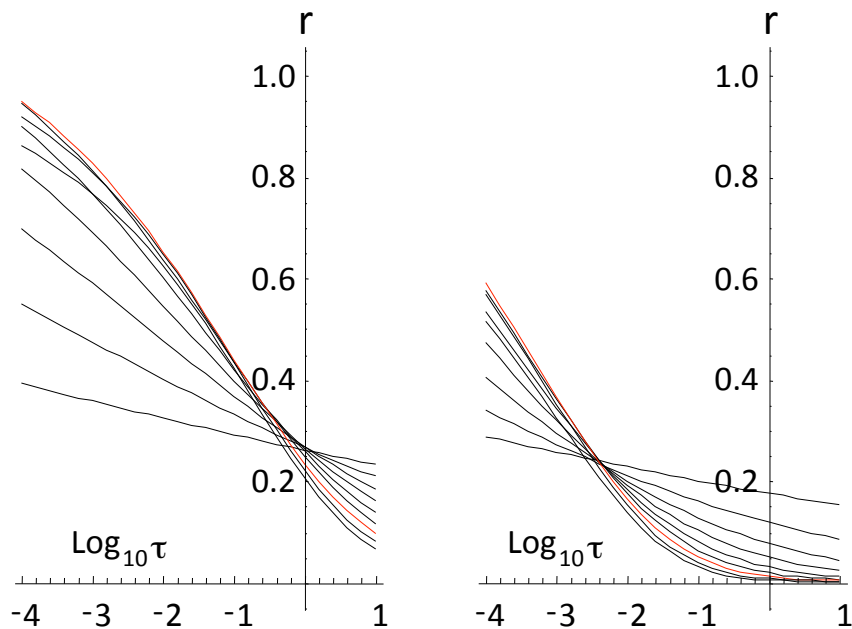
703 To better understand the fGn limit, it is helpful to plot the ratio of the fRn to
 704 fGn skill (fig. 8, right column). We see that even with quite small values $\tau = 10^{-4}$ (top,
 705 black curves), that some skill has already been lost. Fig. 9 shows this more clearly, it
 706 shows one time step and ten time step skill ratios. To put this in perspective, it is
 707 helpful to compare this using some of the parameters relevant to macroweather
 708 forecasting. According to [Lovejoy et al., 2015] and [Del Rio Amador and Lovejoy,



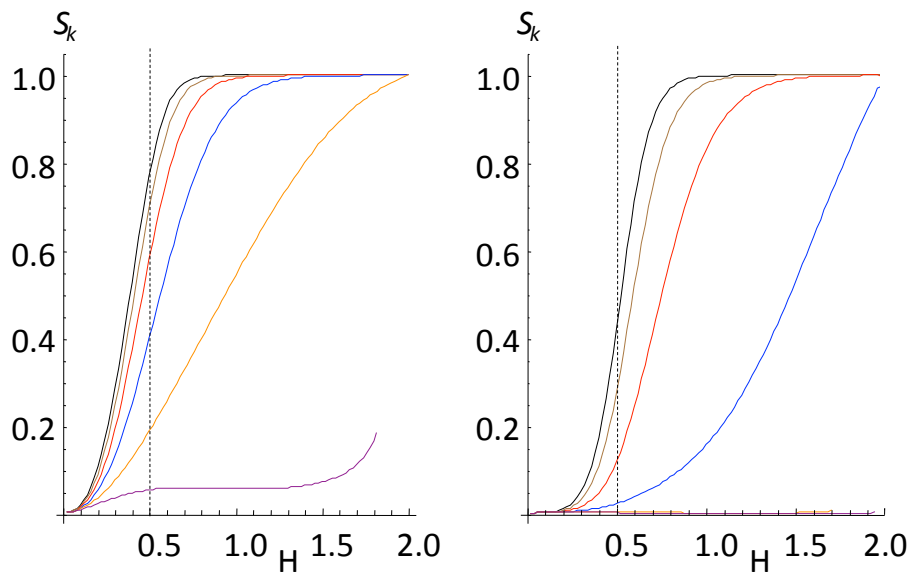
709 2019], the relevant empirical values for the global temperature H is ≈ 0.45 over the
710 range 1 month to 10 years, (i.e. the empirical RMS Haar exponent is ≈ -0.05 so that
711 the $H = -0.05 + 1/2$). Also, according to [Hébert *et al.*, 2019], the transition scale is ≈ 2
712 years (although the uncertainty is large), so that for monthly resolution forecasts,
713 the non-dimensional resolution is $\tau \approx 1/24$. With these values, we see that we may
714 have lost $\approx 25\%$ of the fGn skill for one month forecasts and $\approx 80\%$ for ten month
715 forecasts. Comparing this with fig. 7 we see that this implies about 60% and 10%
716 skill (see also the red curve in fig. 8, bottom set).

717 Going beyond the $0 < H < 1/2$ region that overlaps fGn, fig. 10 clearly shows
718 that the skill continues to increase with H . We already saw (fig. 4) that the range
719 $1/2 < H < 3/2$ has RMS Haar fluctuations that for $\Delta t < 0$ mimic fBm and these do
720 indeed have higher skill, approaching unity for H near 1 corresponding to a Haar
721 exponent $\approx 1/2$, i.e. close to an fBm with $H_B = 1/2$, i.e. a regular Brownian motion.
722 Recall that for Brownian motion, the increments are unpredictable, but the process
723 is predictable (persistence).

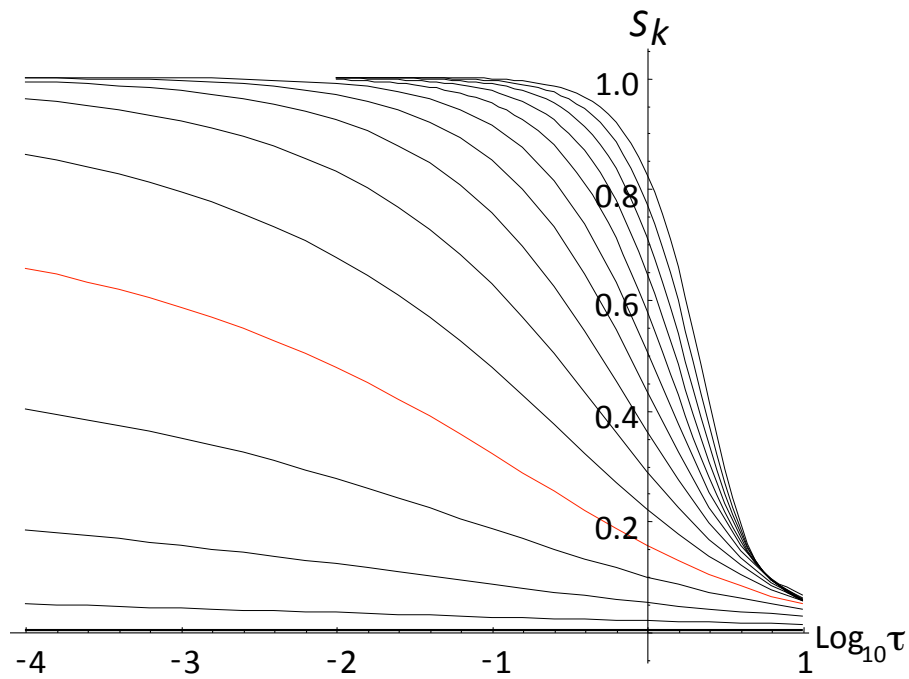
724 Finally, in figure 11a, b, we show the skill for various H 's as a function of
725 resolution τ . Fig. 11a for the $H < 3/2$ shows that for all H , the skill decreases rapidly
726 for $\tau > 1$. Fig. 12b in the fractional oscillation equation regime shows that the skill
727 also oscillates.



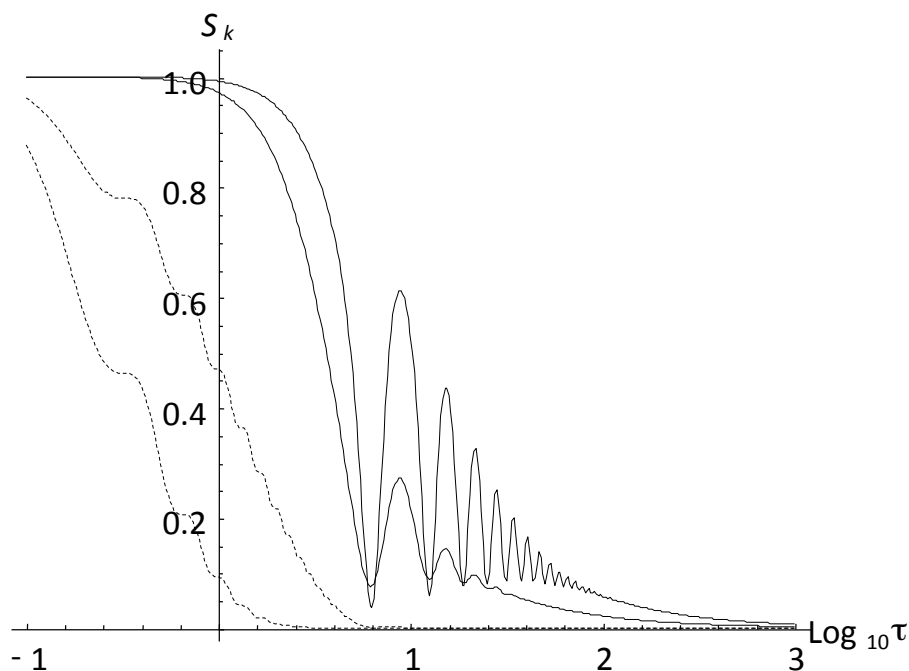
728
729 Fig. 9: The ratio of fRn skill to fGn skill (left: one step horizon, right: ten step
730 forecast horizon) as a function of τ for H increasing from (at left) bottom to top ($H =$
731 $1/20, 2/20, 3/20 \dots 9/20$); the $H = 9/20$ curves is shown in red.



732
733 Fig. 10: The one step (left) and ten step (right) fRn forecast skill as a function of H
734 for various resolutions (τ) ranging from $\tau = 10^{-4}$ (black, left of each set) through to τ
735 = 10 (right of each set, purple, for the right set the $\tau = 1$ (orange), 10 (purple) lines
736 are nearly on top of the $S_k = 0$ line). Recall that the regime $H < 1/2$ (to the left of the
737 vertical dashed lines) corresponds to the overlap with fGn.
738



739
740 Fig. 11a: One step fRn prediction skills as a function of resolution for H 's increasing
741 from $1/20$ (bottom) to $29/20$ (top), every $1/10$. Note the rapid transition to low
742 skill, (white noise) for $\tau > 1$. The curve for $H = 9/20$ is shown in red.



743
744 Fig. 11b: Same as fig. 11a except for $H = 37/20, 39/20$ showing the one step skill
745 (black), and the ten step skill (dashed). The right hand dashed and right hand solid
746 lines, are for $H = 39/20$, they clearly show that the skill oscillates in this fractional
747 oscillation regime. The corresponding left lines are for $H = 37/20$.

748 4. Conclusions:

749 In geophysics, the two main stochastic approaches are stochastic differential
750 equations and stochastic scaling models. In the former, the equations are typically
751 assumed to be of integer order. As a consequence they have exponential Green's
752 functions and they are handled mathematically using the Itô calculus. In contrast,
753 scaling models are typically constructed to directly satisfy scaling symmetries, the
754 usual ones are the linear (monofractal) fBm, fGn and their Levy extensions or the
755 nonlinear stochastic models (cascades, multifractals).

756 In this paper we combine both the scaling and differential equation
757 approaches by allowing the time derivatives to be of fractional order. Fractional
758 derivatives are convolutions with power laws, in Fourier space they are power law
759 filters, they are scaling. In this paper, we considered fractional Langevin equations
760 in which the fractional time (not space) terms are scaling. For technical reasons,
761 these fractional time processes are non-Markovian so that they do not have Fokker-
762 Plank equations nor are they semi-martingales, they are not amenable to the Itô
763 calculus. These technical issues may explain why the stochastic relaxation
764 equations of interest in this paper have barely been considered. Indeed, the closest



765 that have been considered up until now are the stochastic Riemann - Liouville
766 fractional relaxation equations that are relevant in fractional random walks.
767 However, these walks are nonstationary whereas we require stationary processes
768 that are obtained as solutions of stochastic Weyl fractional equations. Our
769 motivation is the proposal by [Lovejoy *et al.*, 2019] that the Fractional Energy
770 Balance Equation (FEBE) is a good model of the earth's radiative equilibrium with
771 the sun and outer space. In this model, the fractional term in the equation
772 phenomenologically accounts for scaling, hierarchical energy storage mechanisms.
773 The deterministic FEBE models the response of the earth to changing external
774 forcings (solar, volcanic, anthropogenic) whereas the noise driven FEBE discussed
775 here models the climate system's response to internal variability that has been
776 acting for a very long time.

777 The FEBE is a fractional relaxation equation that generalizes Newton's law of
778 cooling, it is also a generalization of fractional Gaussian noise (fGn) and its integral
779 fractional Brownian motion (fBm). Over the parameter range $0 < H < 1/2$ (H is the
780 order of the fractional derivative), the high frequency FEBE limit (fGn) has been
781 used as the basis of monthly and seasonal temperature forecasts [Lovejoy *et al.*,
782 2015], [Del Rio Amador and Lovejoy, 2019]. For multidecadal time scales – with the
783 same value $H \approx 0.4$ - it has been used as the basis of climate projections [Hébert *et al.*,
784 2019]. The success of these two applications with a unique exponent makes it
785 plausible that the FEBE is a good model of the earth's energy budget.

786 When the order of the fractional derivative H is in the range $0 < H < 1$, the
787 equation is called the fractional relaxation equation, the value $H = 1$ corresponds to
788 standard integer ordered (exponential) relaxation: for deterministic temperatures it
789 is Newton's law of cooling, for the noise driven case, it yields Ornstein - Uhlenbeck
790 processes. In the range $1 < H < 2$ (the maximum discussed here), the character of
791 the deterministic equation changes, over this range it is called the fractional
792 oscillation equation. In the stochastic case, there are three qualitatively distinct
793 regimes not two: $0 < H < 1/2$, $1/2 < H < 3/2$, $3/2 < H < 2$ with the lower ranges ($0 < H$
794 $< 3/2$) having anomalous high frequency scaling. For example, we found that
795 fluctuations over scales smaller than the relaxation time can either decay or grow
796 with scale - with exponent $H - 1/2$ (section 3.5) - the parameter range $0 < H < 3/2$
797 has the same scaling as the (stationary) fGn ($H < 1/2$) and the (nonstationary) fBm
798 ($1/2 < H < 3/2$), so that processes that have been empirically identified with either
799 fGn or fBm on the basis of their scaling, may in fact turn out to be (stationary) fRn
800 processes; the distinction is only clear at time scales beyond the relaxation time.

801 Since the Riemann-Liouville fractional relaxation equation had already been
802 studied, the main challenge was to implement the Weyl fractional derivative while
803 avoiding divergence issues. The key was to follow the approach used in fBM, i.e. to
804 start by defining fractional motions and then the corresponding noises as the
805 (ordinary) derivatives of the motions. Over the range $0 < H < 1/2$, the noises fGn
806 and fRn diverge in the small scale limit: like Gaussian white noise, they are
807 generalized functions that are strictly only defined under integral signs; they can
808 best be handled as differences of motions.

809 Although the basic approach could be applied to a range of fractional operators,
810 we focused on the fractional relaxation equation. Much of the effort was to deduce



811 the asymptotic small and large scale behaviours of the autocorrelation functions
812 that determine the statistics and in verifying these with extensive numeric
813 simulations. An interesting exception was the $H = 1/2$ special case which for fGn
814 corresponds to an exactly $1/f$ noise. Here, we were able to find exact mathematical
815 expressions for the full correlation functions, showing that they had logarithmic
816 dependencies at both small and large scales. The value $1/2$ is very close to that
817 found empirically for the earth's temperature and the exceptionally slow transition
818 from small to large scales (a factor of a million or more is needed) suggests that this
819 may be a good model for regional temperatures since the variation of the apparent
820 (local) exponents (estimated over a range of 100 to 1000 in scale), may simply be a
821 consequence of varying relaxation time scales rather than regionally varying
822 exponents.

823 **Acknowledgements:**

824 I thank L. Del Rio Amador, R. Procyk and R. Hébert for discussions. I also
825 acknowledge an exchange with N. Watkins and K. Rypdal. This work was unfunded,
826 there were no conflicts of interest.
827



828 **Appendix A: Random walks and the Weyl fractional Relaxation equation**

829 The usual fractional derivatives that are considered in physical applications
 830 are defined over the interval from 0 to t ; this includes the Riemann - Liouville ("R-L";
 831 e.g. the monographs by [Miller and Ross, 1993], and [West et al., 2003]) and the
 832 Caputo fractional derivatives [Podlubny, 1999]. The domain 0 to t is convenient for
 833 initial value problems and can notably be handled by Laplace transform techniques.
 834 However, many geophysical applications involve processes that have started long
 835 ago and are most conveniently treated by derivatives that span the domain $-\infty$ to t ,
 836 i.e. that require the semi-infinite Weyl fractional derivatives.

837 It is therefore of interest to clarify the relationship between the Weyl and R-L
 838 stochastic fractional equations and Green's functions when the systems are driven
 839 by stationary noises. In this appendix, we consider the stochastic fractional
 840 relaxation equation for the velocity V of a diffusing particle. This was discussed by
 841 [Kobelev and Romanov, 2000] and [West et al., 2003] in a physical setting where V
 842 corresponds to the velocity of a fractionally diffusing particle. The fractional
 843 Langevin form of the equation is:

844
$${}_0D_t^H V + V = \gamma \tag{71}$$

845 where γ is a white noise and we have used the R-L fractional derivative. This
 846 equation can be written in a more standard form by integrating both sides by order
 847 H :

848
$$V(t) = -{}_0D_t^{-H} V + {}_0D_t^{-H} \gamma = -\frac{1}{\Gamma(H)} \int_0^t (t-s)^{H-1} V(s) ds + \frac{1}{\Gamma(H)} \int_0^t (t-s)^{H-1} \gamma(s) ds \tag{72}$$

849 The position $X(t) = \int_0^t V(s) ds + X_0$ satisfies:

850
$${}_0D_t^H X + X = W \tag{73}$$

851 where $dW = \gamma(s) ds$ is a Wiener process.

852 The solution for $X(t)$ is obtained using the Green's function $G_{0,H}$:

853
$$X(t) = \int_0^t G_{0,H}(t-s) W(s) ds + X_0 E_{1,H}(-t^H); \quad G_{0,H}(t) = t^{H-1} E_{H,H}(-t^H) \tag{74}$$

854 where E is a Mittag-Leffler function (eq. 16). Integrating by parts and using $G_{1,H}(0)$
 855 = 0, $W(0) = 0$ we obtain:

856
$$\int_0^t G_{0,H}(t-s) W(s) ds = \int_0^t G_{1,H}(t-s) \gamma(s) ds; \quad dW = \gamma(s) ds; \quad G_{1,H}(t) = \int_0^t G_{0,H}(s) ds \tag{75}$$

857 This yields:

858
$$X(t) = \int_0^t G_{1,H}(t-s) \gamma(s) ds + X_0 E_{1,H}(-t^H) \tag{76}$$



859 $X(t)$ is clearly nonstationary: its statistics depend strongly on t . The first step in
 860 extracting a stationary process is to take the limit of very large t , and consider the
 861 process over intervals that are much shorter than the time since the particle began
 862 diffusing. We will show that the increments of this new process are stationary.

863 Define the new process $Z_{t'}(t)$ over a time interval t that is short compared to
 864 the time elapsed since the beginning of the diffusion (t'):

$$865 \quad Z_{t'}(t) = X(t') - X(t' - t) = \int_0^{t'} G_{0,H}(t' - s) \gamma(s) ds - \int_0^{t'-t} G_{0,H}(t' - t - s) \gamma(s) ds \quad (77)$$

866 (for simplicity we will take $X_0 = 0$, but since $E_{1,H}(-t'^H)$ rapidly decreases to zero, at
 867 large t' this is not important). Now use the change of variable $s' = s - t' + t$:

$$868 \quad Z_{t'}(t) = \int_{-t'+t}^t G_{1,H}(t - s') \gamma(s' + t' - t) ds' - \int_{-t'+t}^0 G_{1,H}(-s') \gamma(s' + t' - t) ds' \quad (78)$$

869 Now, use the fact that $\gamma(s' + t' - t) = \gamma(s')$ (equality in a probability sense) and take
 870 the limit $t' \rightarrow \infty$. Dropping the prime on s we can write this as:

$$871 \quad Z(t) = Z_{\infty}(t) = \int_{-\infty}^t G_{1,H}(t - s) \gamma(s) ds - \int_{-\infty}^0 G_{1,H}(-s) \gamma(s) ds \quad (79)$$

872 where we have written $Z(t)$ for the limiting process.

873 Since $Z(0) = 0$, $Z(t)$ is still nonstationary. But now consider the process $Y(t)$
 874 given by its derivative:

$$875 \quad Y(t) = \frac{dZ(t)}{dt} = \int_{-\infty}^t G_{0,H}(t - s) \gamma(s) ds; \quad G_{0,H}(t) = \frac{dG_{1,H}(t)}{dt} \quad (80)$$

876 (since $G_1(0) = 0$). $Y(t)$ is clearly stationary.

877 We now show that $Y(t)$ satisfies the Weyl version of the relaxation equation.

878 Consider the shifted function: $Y_{t'}(t) = Y_0(t + t')$ and take Y_0 as a solution to the
 879 Riemann-Liouville fractional equation:

$$880 \quad {}_0 D_t^H Y_0 + Y_0 = \gamma \quad (81)$$

881 or equivalently in integral form:

$$882 \quad Y_0(t) = -{}_0 D_t^{-H} Y_0 + {}_0 D_t^{-H} \gamma = -\frac{1}{\Gamma(H)} \int_0^t (t-s)^{H-1} Y_0(s) ds + \frac{1}{\Gamma(H)} \int_0^t (t-s)^{H-1} \gamma(s) ds \quad (82)$$

883 With solution:

$$884 \quad Y_0(t) = \int_0^t G_{0,H}(t-s) \gamma(s) ds \quad (83)$$

885 (with $Y_0(0) = 0$).

886 Now shift the time variable so as to obtain:



$$Y_{t'}(t) = -\frac{1}{\Gamma(H)} \int_0^{t+t'} (t+t'-s)^{H-1} Y_0(s) ds + \frac{1}{\Gamma(H)} \int_0^{t+t'} (t+t'-s)^{H-1} \gamma(s) ds \quad (84)$$

(with $Y_{t'}(-t') = 0$). Now make the change of variable $s' = s - t'$:

$$Y_{t'}(t) = -\frac{1}{\Gamma(H)} \int_{-t'}^t (t-s')^{H-1} Y_{t'}(s') ds' + \frac{1}{\Gamma(H)} \int_{-t'}^t (t-s')^{H-1} \gamma(s') ds'; \quad \gamma(s'+t') = \gamma(s') \quad (85)$$

We see that $Y_{t'}$ is therefore the solution of:

$${}_{-t'}D_t^H Y_{t'} + Y_{t'} = \gamma \quad (86)$$

However, since $Y_{t'}$ is the shifted Y_0 we have the solution:

$$Y_{t'}(t) = Y_0(t+t') = \int_0^{t+t'} G_0(t+t'-s) \gamma(s) ds = \int_{-t'}^t G_0(t-s') \gamma(s'+t') ds' \quad (87)$$

Again, using $\gamma(s'+t') = \gamma(s')$ and dropping the primes, we obtain:

$$Y_{t'}(t) = \int_{-t'}^t G_0(t-s) \gamma(s) ds \quad (88)$$

Finally, taking the limit $t' \rightarrow \infty$ we have the equation and solution for $Y(t) = Y_\infty(t)$:

$${}_{-\infty}D_t^H Y + Y = \gamma; \quad Y(t) = \int_{-\infty}^t G_0(t-s) \gamma(s) ds; \quad Y(t) = Y_\infty(t) \quad (89)$$

with $Y(-\infty) = 0$.

The conclusion is that as long as the forcings are statistically stationary we can use the R-L Green's functions to solve the Weyl fractional derivative equation. Although we have explicitly derived the result for the fractional relaxation equation, we can see that it is of wider generality.



904 **Appendix B: The small and large scale fRn, fRm statistics:**

905 **B.1 Discussion**

906 In section 2.3, we derived general statistical formulae for the auto-correlation
 907 functions of motions and noises defined in terms of Green's functions of fractional
 908 operators. Since the processes are Gaussian, autocorrelations fully determine the
 909 statistics. While the autocorrelations of fBm and fGn are well known (and discussed
 910 in section 3.1), those for fRm and fRn are new and are not so easy to deal with since
 911 they involve quadratic integrals of Mittag-Leffler functions.

912 In this appendix, we derive the leading terms in the basic small and large t
 913 expansions, including results of Padé approximants that provide accurate
 914 approximations to fRn at small times.

915 **B.2 Small t behaviour**

916 **fRn statistics:**

917 a) The range $0 < H < 1/2$:

918 Start with:

$$919 \quad R_H(t) = N_H^2 \int_0^\infty G_{0,H}(t+s) G_{0,H}(s) ds \quad (90)$$

920 (eq. 34) and use the series expansion for $G_{0,H}$:

$$921 \quad G_{0,H}(s) = \sum_{n=0}^{\infty} (-1)^{n+1} \frac{s^{(n+1)H-1}}{\Gamma(n+1)} \quad (91)$$

922 So that:

$$923 \quad R_H(t) = N_H^2 \sum_{n,m=0}^{\infty} \frac{(-1)^{n+m}}{\Gamma(n+1)\Gamma(m+1)} \int_0^\infty (s+t)^{(n+1)H-1} s^{(m+1)H-1} ds \quad (92)$$

924 This can be written:

$$925 \quad R_H(t) = N_H^2 t^{-1+2H} \sum_{n,m=0}^{\infty} A_{nm} t^{(m+n)H}; \quad A_{nm} = \frac{(-1)^{n+m}}{\Gamma(n+1)\Gamma(m+1)} \int_0^\infty (1+\xi)^{(n+1)H-1} \xi^{(m+1)H-1} d\xi \quad (93)$$

926 Evaluating the integral, and changing summation variables, we obtain:

927

$$928 \quad A_{km} = \frac{(-1)^k \Gamma(1-H(k+2)) \sin(H\pi(m+1))}{\pi}; \quad k = m+n; \quad k < \left[\frac{1}{H} \right] - 2 \quad (94)$$

929 where we have taken $k = n + m$ and the square brackets indicate the integer
 930 part; beyond the indicated k range, the integrals diverge at infinity.

931 We can now sum over m :



$$R_H(t) = N_H^2 t^{-1+2H} \sum_{k=0}^{\left[\frac{1}{H}\right]-2} B_k t^{kH}; \quad B_k = (-1)^k \frac{\Gamma(1-H(k+2)) \sin\left(H(k+1)\frac{\pi}{2}\right) \sin\left(H(k+2)\frac{\pi}{2}\right)}{\pi \sin\left(H\frac{\pi}{2}\right)}$$

932
 933

where we have used:

$$\sum_{m=0}^{k+1} \sin(H\pi(m+1)) = \frac{\sin\left(H(k+1)\frac{\pi}{2}\right) \sin\left(H(k+2)\frac{\pi}{2}\right)}{\sin\left(H\frac{\pi}{2}\right)}$$

934
 935

Finally, we can introduce the polynomial $f(z)$ and write:

$$R_H(t) = N_H^2 t^{-1+2H} f(t^H); \quad f(z) = \sum_{k=0}^{\left[\frac{1}{H}\right]-2} B_k z^k$$

936
 937

Taking the $k = 0$ term only and using the $H < 1/2$ normalization $N_H = K_H$, we have

938

$K_H^2 B_0 = H(1+2H)$ and (as expected), we obtain the fGn result:

$$R_H(t) = H(1+2H)t^{-1+2H} + O(t^{-1+3H}); \quad t \ll 1; \quad 0 < H < 1/2$$

939
 940

(for t larger than the resolution τ).

941
 942
 943
 944
 945

Since the series is divergent, the accuracy decreases if we use more than one term in the sum. The series is nevertheless useful because the terms can be used to determine Padé approximants, and they can be quite accurate (see fig. B1 and the discussion below). The approximant of order 1, 2 was found to work very well over the whole range $0 < H < 3/2$.

946
 947

b) The range $1/2 < H < 3/2$:

948
 949

In this range, no terms in the expansion eq. 97 converge, however, the series still turns out to be useful. To see this use the identity:

$$2(1 - R_H(t)) = N_H^2 \int_0^\infty (G_{0,H}(s+t) - G_{0,H}(s))^2 ds + N_H^2 \int_0^t G_{0,H}(s)^2 ds; \quad N_H = C_H^{-1}; \quad H > 1/2$$

950
 951

where we have used the $H > 1/2$ normalization $N_H = 1/C_H$.

952
 953
 954
 955

It turns out that if use this identity and substitute the series expansion for $G_{0,H}$, that the integrals converge up until order $m+n < [3/H] - 2$ (rather than $[1/H] - 2$), and the coefficients are identical. We obtain:

$$R_H(t) = 1 - N_H^2 t^{-1+2H} f(t^H); \quad f(z) = \sum_{k=0}^{\left[\frac{3}{H}\right]-1} B_k z^k; \quad 1/2 < H < 3/2$$

956
 957
 958

where the B_k are the same as before. This formula is very close to the one for $0 < H < 1/2$ (eq. 97).



959

960 c) The range $3/2 < H < 2$:

961 Again using the identity eq. 99, we can make the approximation

962 $G_{0,H}(s+t) - G_{0,H}(s) \approx tG'_{0,H}(s)$; this is useful since when $H > 3/2$, $\int_0^\infty G'_{0,H}(s)^2 ds < \infty$ and

963 we obtain:

$$964 \quad R_H(t) = 1 - \frac{t^2}{2C_H^2} \int_0^\infty G'_{0,H}(s)^2 ds + O(t^{2H-1}); \quad 3/2 < H < 2 \quad (101)$$

965

966 **Padé:**

967 Although the series (eqs. 97, 100) diverge, they can still be used to determine
 968 Padé approximants (see e.g. [Bender and Orszag, 1978]). Padé approximants are
 969 rational functions such that the first $N + M + 1$ of their Taylor expansions of are the
 970 same as the first $N + M + 1$ coefficients of the function f to which they approximate.
 971 The optimum (for $H < 1/4$) is the $N = 1, M = 2$ approximant ("Padé 12", denoted P_{12}).
 972 Applied to the function $f(z)$ in eq. 97, its first four terms are:

973

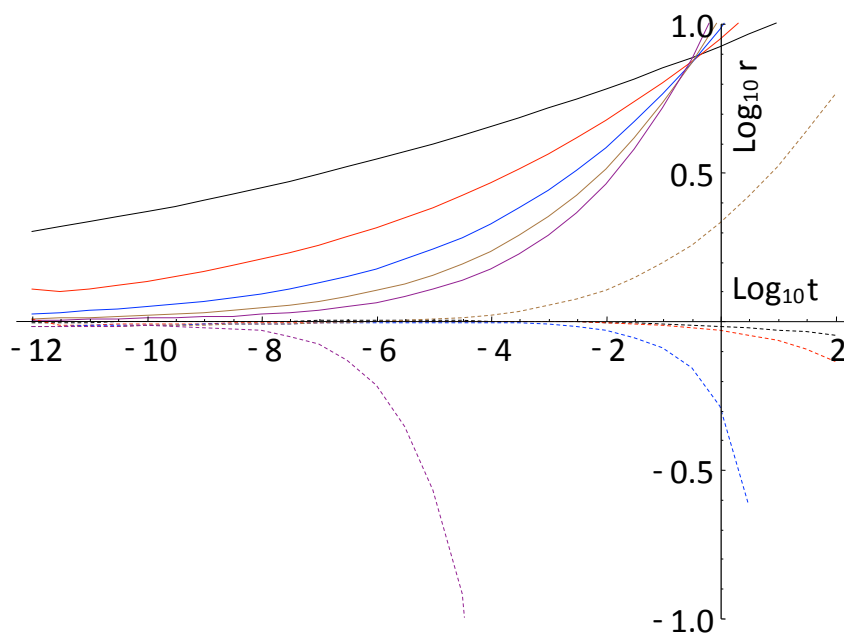
$$974 \quad f(z) = B_0 + B_1 z + B_2 z^2 + B_3 z^3 \quad (102)$$

975

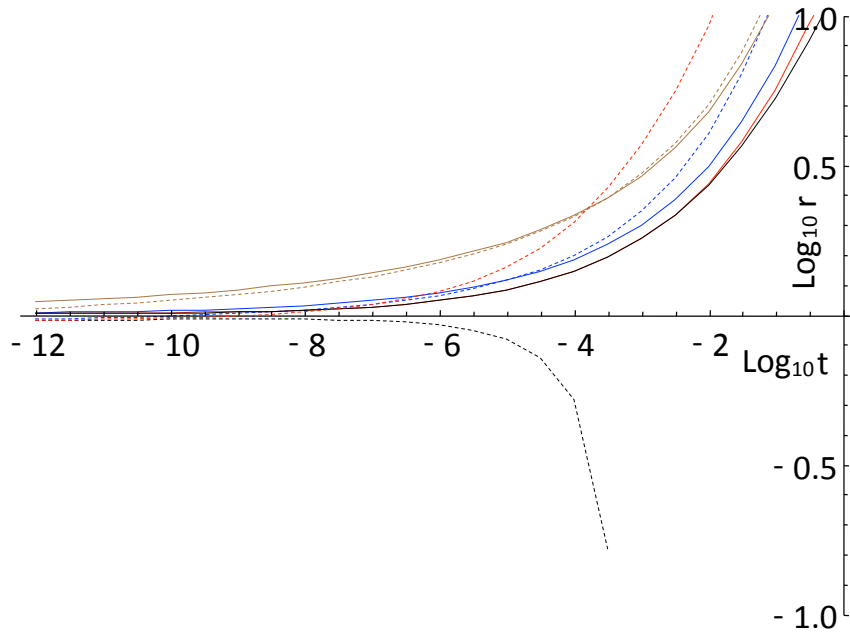
976 with approximant:

$$977 \quad P_{12}(z) = \frac{B_0(B_1^2 - B_0 B_2) + z(B_1^3 - 2B_0 B_1 B_2 + B_0^2 B_3)}{B_0 B_2 - B_1^2 + z(B_0 B_3 - B_1 B_2) + z^2(B_1 B_3 - B_2^2)} \quad (103)$$

978 where the B_k are taken from the expansion eq. 95. Figures B1, B2 show that the
 979 approximants are especially accurate in the lower range of H values where the first
 980 term in the series (the fGn approximation) is particularly poor.



981
982 Fig. B1: The \log_{10} ratio of the fRn correlation function $R^{(fRn)}_H(t)$ to the fGn
983 approximation $R^{(fGn)}_H(t)$ (solid) and to the Padé approximant $R^{(Padé)}_H(t)$ (dashed) for
984 $H = 1/20$ (black), $2/20$ (red), $3/20$ (blue), $4/20$ (brown), $5/20$ (purple). The Padé
985 approximant is the Padé12 polynomial (eq. 103). As H increases to 0.25, Pade gets
986 worse, fGn gets better (see fig. B2).



987
 988 Fig. B2: The same as fig. B1 but for $H = 6/20$ (brown), $7/20$ (blue), $8/20$ (red), $9/20$
 989 (black). The Padé12 approximant (dashed) is generally a bit worse than fGn
 990 approximation (solid).

991
 992 **fRm statistics:**

993 For the small t behaviour of the motion fRm, it is simplest to integrate $R_H(t)$
 994 twice:

$$995 \quad V_H(t) = 2 \int_0^t \left(\int_0^s R_H(p) dp \right) ds \quad (104)$$

996 using the expansion eq. 95, we obtain:

$$997 \quad V_H(t) = K_H^2 t^{1+2H} \sum_{k=0}^{\lfloor \frac{1}{H} \rfloor - 2} \frac{B_k}{H(k+2)(1+H(k+2))} t^{kH}; \quad 0 < H < 1/2$$

$$998 \quad V_H(t) = t^2 - C_H^{-2} t^{1+2H} \sum_{k=0}^{\lfloor \frac{3}{H} \rfloor - 2} \frac{B_k}{H(k+2)(1+H(k+2))} t^{kH}; \quad 1/2 < H < 3/2$$

(105)

999 the leading terms are:



1000 $V_H(t) = t^{1+2H} + O(t^{1+3H}); \quad 0 < H < 1/2$ (106)
 1001 (106)
 1002 and:

1003 $V_H(t) = t^2 - \frac{\Gamma(-1-2H)\sin(\pi H)}{\pi C_H^2} t^{1+2H} + O(t^{1+3H}); \quad 1/2 < H < 3/2$ (107)
 1004 (107)
 1005 To find an expansion for the range $3/2 < H < 2$, we similarly integrate eq. 101:

1006 $V_H(t) = t^2 - \frac{t^4}{12C_H^2} \int_0^\infty G'_{0,H}(s)^2 ds + O(t^{2H+1}); \quad 3/2 < H < 2$ (108)

1007 **B.3 Large t behaviour:**

1008 When t is large, we can use the asymptotic t expansion:
 1009

1010 $G_{1,H}(t) = 1 + \sum_{m=1}^{\infty} \frac{(-1)^m}{m\Gamma(1-mH)} t^{-mH}$ (109)

1011 to evaluate the first integral on the right in eq. 23. Using eq. 109 for the $G_{1,H}(s+t)$
 1012 term and the usual series expansion for the $G_{1,H}(s)$ we see that we obtain terms of
 1013 the type:

1014 $\int_0^\infty (s+t)^{-mH} s^{nH} ds \propto t^{1-(m-n)H}; \quad (m-n)H > 1$ (110)

1015 there will only be terms of decreasing order (the unit term has no t dependence).

1016 Now consider the second integral in eq. 23:

1017 $I_2 = \int_0^t G_{1,H}(s)^2 ds \approx \int_0^t \left(1 - \frac{2s^{-H}}{\Gamma(1-H)} + \dots \right) ds \approx t - \frac{2t^{1-H}}{\Gamma(2-H)} + O(t^{1-2H}); \quad t \gg 1$ (111)

1018 As long as $H < 1$, both of these terms will increase with t and will therefore dominate
 1019 the first term: they will thus be the leading terms. We therefore obtain the
 1020 expansion:

1021 $V_H(t) = N_H^2 \left[t - \frac{2t^{1-H}}{\Gamma(2-H)} + a_H + O(t^{1-2H}) \right]$ (112)

1022 where a_H is a constant term from the first integral. Putting the terms in leading
 1023 order, depending on the value of H :



1024
$$V_H(t) = N_H^2 \left[t - \frac{2t^{1-H}}{\Gamma(2-H)} + a_H + O(t^{1-2H}) \right]; \quad H < 1$$

1025
$$V_H(t) = N_H^2 \left[t + a_H - \frac{2t^{1-H}}{\Gamma(2-H)} + O(t^{1-2H}) \right]; \quad H > 1$$

(113)

1025 To determine $R_H(t)$ we simply differentiate twice and multiply by $\frac{1}{2}$:

1026
$$R_H(t) = -N_H^2 \left[\frac{t^{-1-H}}{\Gamma(-H)} + O(t^{-1-2H}) \right]; \quad 0 < H < 2$$

(114)

1027 Note that for $0 < H < 1$, $\Gamma(-H) < 0$ so that $R > 0$ over this range.

1028 All the formulae for both the small and large t behaviours were verified
1029 numerically; see figs. 2, 3, 4.

1030



1031 **Appendix C: The $H=1/2$ special case:**

1032 When $H = 1/2$, the high frequency fGn limit is an exact “1/f noise”, (spectrum
 1033 ω^{-1}) it has both high and low frequency divergences. The high frequency divergence
 1034 can be tamed by averaging, but the not the low frequency divergence, so that fGn is
 1035 only defined for $H < 1/2$. However, for the fRn, the low frequencies are convergent
 1036 (appendix B) over the whole range $0 < H < 2$, and we find that the correlation
 1037 function has a logarithmic dependence at both small and large scales. This is
 1038 associated with particularly slow transitions from high to low frequency behaviours.
 1039 The critical value $H = 1/2$ is thus of intrinsic interest; and for fRn, it is possible to
 1040 obtain exact analytic expressions for R_H , V_H and the Haar fluctuations; we develop
 1041 these in this appendix. For simplicity, we assume the normalization $N_H = 1$.

1042 The starting point is the expression:

$$E_{1/2,1/2}(-z) = \frac{1}{\sqrt{\pi}} - ze^{z^2} \operatorname{erfc}(z) \quad \operatorname{erfc}(z) = \frac{2}{\sqrt{\pi}} \int_z^\infty e^{-s^2} ds$$

$$E_{1/2,3/2}(-z) = \frac{1 - e^{z^2} \operatorname{erfc}(z)}{z} \quad (115)$$

1043 (e.g. [Podlubny, 1999]). From this, we obtain the impulse and step Green’s
 1044 functions:
 1045

$$G_{0,1/2}(t) = \frac{1}{\sqrt{\pi t}} - e^t \operatorname{erfc}(t^{1/2})$$

$$G_{1,1/2}(t) = 1 - e^t \operatorname{erfc}(t^{1/2}) \quad (116)$$

1046 (see eq. 16). The impulse response $G_{0,H}(t)$ can be written as a Laplace transform:

$$G_{0,1/2}(t) = \frac{1}{\pi} \int_0^\infty \frac{\sqrt{p}}{1+p} e^{-tp} dp \quad (117)$$

1048 Therefore, the correlation function is:

$$R_{1/2}(t) = \int_0^\infty G_{0,1/2}(t+s) G_{0,1/2}(s) ds = \frac{1}{\pi^2} \int_0^\infty ds e^{-s(p+q)} \int_0^\infty \int_0^\infty \frac{\sqrt{qp}}{(1+p)(1+q)} e^{-qt} dp dq \quad (118)$$

1050 Performing the s and p integrals we have:

$$R_{1/2}(t) = \frac{1}{2\pi} \int_0^\infty \left[\frac{1}{(1+q)} + \frac{\sqrt{q}}{(1+q)} - \frac{1}{(1+\sqrt{q})} \right] e^{-qt} dq \quad (119)$$

1051 Finally, this Laplace transform yields:

$$R_{1/2}(t) = \frac{1}{2} \left(e^{-t} \operatorname{erfi} \sqrt{t} - e^t \operatorname{erfc} \sqrt{t} \right) - \frac{1}{2\pi} \left(e^t \operatorname{Ei}(-t) + e^{-t} \operatorname{Ei}(t) \right) \quad (120)$$

1052 where:

$$Ei(z) = - \int_{-z}^\infty \frac{e^{-u}}{u} du \quad (121)$$

1056



1057 and:

$$\operatorname{erfi}(z) = -i(\operatorname{erf}(iz)); \quad \operatorname{erf}(z) = \frac{2}{\sqrt{\pi}} \int_0^z e^{-s^2} ds$$

1058 (122)

1059 To obtain the corresponding V_H use:

$$V_{1/2}(t) = 2 \int_0^t \left(\int_0^s R_{1/2}(p) dp \right) ds$$

1060 (123)

1061 The exact $V_{1/2}(t)$ is:

$$V_{1/2}(t) = G_{3,4}^{2,2} \left[\begin{matrix} 2, 2, 5/2 \\ 2, 2, 0, 5/2 \end{matrix} \right] + \frac{e^t}{\pi} (\operatorname{Shi}(t) - \operatorname{Chi}(t)) + (e^{-t} \operatorname{erfi}(\sqrt{t}) - e^t \operatorname{erf}(\sqrt{t}))$$

$$+ t \left(1 + \frac{\gamma_E - 1}{\pi} \right) - 4\sqrt{\frac{t}{\pi}} + \frac{(1+t) \log t}{\pi} + 1 + \frac{\gamma_E}{\pi}$$

1062 (124)

1064 where $G_{3,4}^{2,2}$ is the MeijerG function, Chi is the CoshIntegral function and Shi is the
 1065 SinhIntegral function.

1066 We can use these results to obtain small and large t expansions:

$$R_{1/2}(t) = - \left(\frac{2\gamma_E + \pi + 2 \log t}{2\pi} \right) + \frac{2\sqrt{t}}{\sqrt{\pi}} - \frac{t}{2} - \left(\frac{3 + 2\gamma_E + \pi + 2 \log t}{4\pi} \right) t^2 + O(t^{3/2}); \quad t \ll 1$$

1067 (125)

$$R_{1/2}(t) = \frac{1}{2\sqrt{\pi}} t^{-3/2} - \frac{1}{\pi} t^{-2} + \frac{15}{8\sqrt{\pi}} t^{-7/2} + O(t^{-4}); \quad t \gg 1$$

1068
 1069

1070 where γ_E is Euler's constant = 0.57... and:

$$V_{1/2}(t) = - \frac{t^2 \log t}{\pi} + \frac{191 - 156\gamma_E - 78\pi}{144\pi} + \frac{16}{15\sqrt{\pi}} t^{5/2} - \frac{t^3}{6} - \frac{t^4 \log t}{12\pi} + O(t^{3/2}); \quad t \ll 1$$

1071 (126)

$$V_{1/2}(t) = t + \frac{\pi + 2\gamma_E}{\pi} + \frac{2 \log t}{\pi} - \frac{4}{\sqrt{\pi}} t^{1/2} + \frac{1}{\sqrt{\pi}} t^{-1/2} - \frac{2}{\pi} t^{-2} + \frac{15}{4\sqrt{\pi}} t^{-3/2} + O(t^{-4}); \quad t \gg 1$$

1072
 1073

We can also work out the variance of the Haar fluctuations:

$$\langle \Delta U_{1/2}^2(\Delta t) \rangle = \frac{\Delta t^2 \log \Delta t}{4\pi} + \frac{6\pi + 12\gamma_E - \log 16 + 960 \log 2}{240\pi} + \frac{512(\sqrt{2} - 2)}{240\sqrt{\pi}} \Delta t^{1/2} + \frac{\Delta t}{3} + O(\Delta t^{3/2}); \quad \Delta t \ll 1$$

1074 (127)

1075

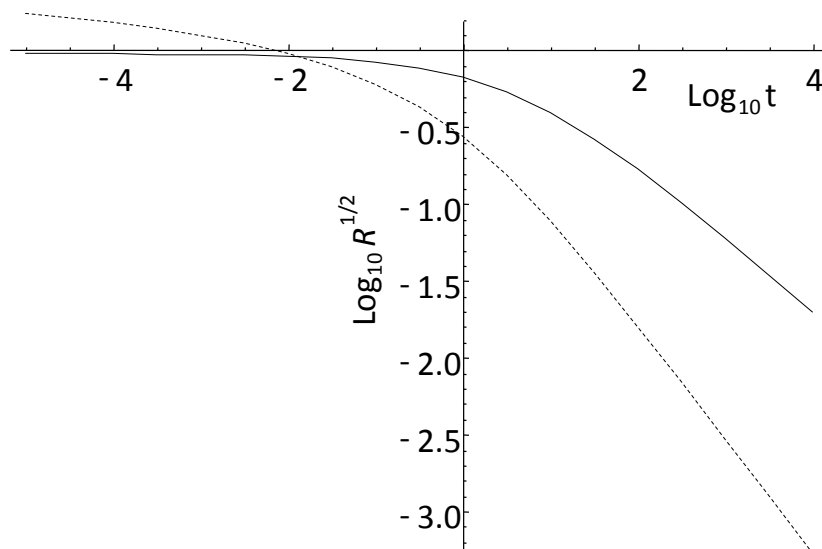
$$\langle \Delta U_{1/2}^2(\Delta t) \rangle = 4\Delta t^{-1} - \frac{32\sqrt{2}}{\sqrt{\pi}} \Delta t^{-3/2} + \frac{3t^{-2} \log \Delta t}{\pi} + O(\Delta t^{-2}); \quad \Delta t \gg 1$$

1076
 1077
 1078

Figure C1 shows numerical results for the fRn with $H = 1/2$, the transition between small and large t behaviour is extremely slow; the 9 orders of magnitude



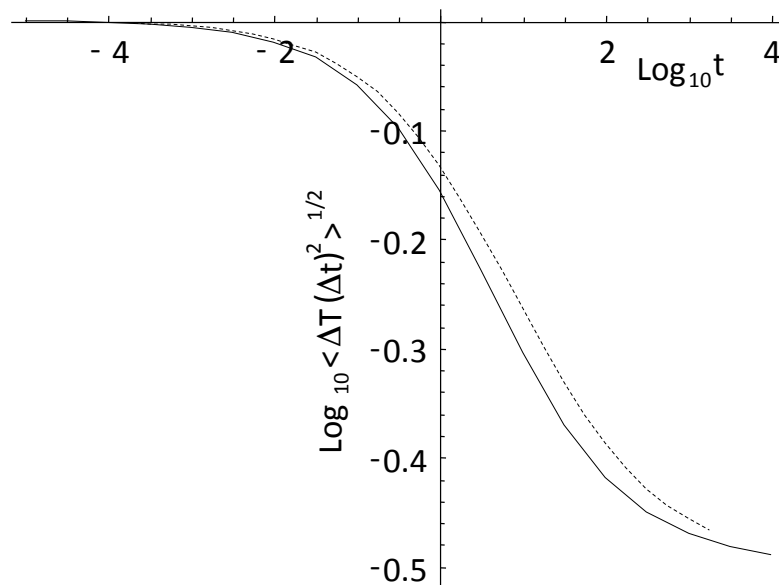
1079 depicted in the figure are barely enough. The extreme low $(R_{1/2})^{1/2}$ (dashed)
1080 asymptotes at the left to a slope zero (a square root logarithmic limit, eq. 125), and
1081 to a $-3/4$ slope at the right. The RMS Haar fluctuation (black) changes slope from 0
1082 to $-1/2$ (left to right). This is shown more clearly in fig. C2 that shows the
1083 logarithmic derivative of the RMS Haar (black) compared to a regression estimate
1084 over two orders of magnitude in scale (blue; a factor 10 smaller and 10 larger than
1085 the indicated scale was used). This figure underlines the gradualness of the
1086 transition from $H = 0$ to $H = -1/2$. If empirical data were available only over a factor
1087 of 100 in scale, depending on where this scale was with respect to the relaxation
1088 time scale (unity in the plot), the RMS Haar fluctuations could have any slope in the
1089 range 0 to $-1/2$ with only small deviations.



1090 Fig. C1: fR_n statistics for $H = 1/2$: the solid line is the RMS Haar fluctuation, the
1091 dashed line is the root correlation function $(R_{1/2})^{1/2}$ (the normalization constant = 1,
1092 it has a logarithmic divergence at small t).
1093



50



1094
1095 Fig. C2: The logarithmic derivative of the RMS Haar fluctuations (solid) in fig. C1
1096 compared to a regression estimate over two orders of magnitude in scale (dashed; a
1097 factor 10 smaller and 10 larger than the indicated scale was used). This plot
1098 underlines the gradualness of the transition from $H = 0$ to $H = -1/2$: over range of
1099 100 or so in scale there is approximate scaling but with exponents that depend on
1100 the range of scales covered by the data. If data were available only over a factor of
1101 100 in scale, the RMS Haar fluctuations could have any slope in the fGn range 0 to
1102 $-1/2$ with only small deviations.
1103



1104
1105

1106 **References:**

- 1107 Bender, C. M., and Orszag, S. A., *Advanced mathematical methods for scientists and*
1108 *engineers*, Mc Graw Hill, 1978.
- 1109 Biagini, F., Hu, Y., Øksendal, B., and Zhang, T., *Stochastic Calculus for Fractional*
1110 *Brownian Motion and Applications*, Springer-Verlag, 2008.
- 1111 Buizza, R., Miller, M., and Palmer, T. N., Stochastic representation of model
1112 uncertainties in the ECMWF Ensemble Prediction System, *Q. J. Roy. Meteor. Soc.*,
1113 125, 2887–2908, 1999.
- 1114 Chekroun, M. D., Simonnet, E., and Ghil, M., Stochastic Climate Dynamics: Random
1115 Attractors and Time-dependent Invariant Measures *Physica D*, 240, 1685-1700
1116 2010.
- 1117 Del Rio Amador, L., and Lovejoy, S., Predicting the global temperature with the
1118 Stochastic Seasonal to Interannual Prediction System (StocSIPS) *Clim. Dyn.* doi:
1119 org/10.1007/s00382-019-04791-4., 2019.
- 1120 Dijkstra, H., *Nonlinear Climate Dynamics*, 357 pp., Cambridge University Press, 2013.
- 1121 Gripenberg, G., and Norros, I., On the Prediction of Fractional Brownian Motion *J.*
1122 *Appl. Prob.*, 33, 400-410, 1996.
- 1123 Hébert, R., Lovejoy, S., and Tremblay, B., An Observation-based Scaling Model for
1124 Climate Sensitivity Estimates and Global Projections to 2100, *Climate Dynamics*,
1125 (under revision), 2019.
- 1126 Hurst, H. E., Long-term storage capacity of reservoirs, *Transactions of the American*
1127 *Society of Civil Engineers*, 116, 770-808, 1951.
- 1128 Jumarie, G., Stochastic differential equations with fractional Brownian motion inputs,
1129 *Int. J. Systems. Sci.*, 24, 1113, 1993.
- 1130 Karczewska, A., and Lizama, C., Solutions to stochastic fractional relaxation
1131 equations, *Phys. Scr.*, T136 7pp doi: 10.1088/0031-8949/2009/T136/014030
1132 2009.
- 1133 Kobelev, V., and Romanov, E., Fractional Langevin Equation to Describe Anomalous
1134 Diffusion *Prog. of Theor. Physics Supp.*, 139, 470-476, 2000.
- 1135 Lovejoy, S., and Schertzer, D., *The Weather and Climate: Emergent Laws and*
1136 *Multifractal Cascades*, 496 pp., Cambridge University Press, 2013.
- 1137 Lovejoy, S., del Rio Amador, L., and Hébert, R., The ScaLIing Macroweather Model
1138 (SLIMM): using scaling to forecast global-scale macroweather from months to
1139 Decades, *Earth Syst. Dynam.*, 6, 1–22 doi: [http://www.earth-syst-](http://www.earth-syst-dynam.net/6/1/2015/)
1140 [dynam.net/6/1/2015/](http://www.earth-syst-dynam.net/6/1/2015/), doi:10.5194/esd-6-1-2015, 2015.
- 1141 Lovejoy, S., Procyk, R., del Rio Amador, L., and Hébert, R., The fractional Energy
1142 Balance Equation, *Earth Syst. Dyn. Disc.*, (in preparation), 2019.
- 1143 Mandelbrot, B. B., *The Fractal Geometry of Nature*, Freeman, 1982.
- 1144 Mandelbrot, B. B., and Van Ness, J. W., Fractional Brownian motions, fractional
1145 noises and applications, *SIAM Review*, 10, 422-450, 1968.
- 1146 Miller, K. S., and Ross, B., *An introduction tyo the fractional calculus and fractional*
1147 *differential equations*, 366 pp., John Wiley and Sons, 1993.



- 1148 Papoulis, A., *Probability, Random Variables and Stochastic Processes*, Mc Graw Hill,
1149 1965.
- 1150 Podlubny, I., *Fractional Differential Equations*, 340 pp., Academic Press, 1999.
- 1151 Schertzer, D., and Lovejoy, S., Physical modeling and Analysis of Rain and Clouds by
1152 Anisotropic Scaling of Multiplicative Processes, *Journal of Geophysical Research*,
1153 92, 9693-9714, 1987.
- 1154 Schertzer, D., Larchevue, M., Duan, J., Yanovsky, V. V., and Lovejoy, S., Fractional
1155 Fokker-Planck equation for nonlinear stochastic differential equation driven
1156 by non-Gaussian Levy stable noises, *J. of Math. Physics*, 42, 200-212, 2001.
- 1157 West, B. J., Bologna, M., and Grigolin, P., *Physics of Fractal Operators*, 354 pp.,
1158 Springer, 2003.
- 1159